HHS Public Access

Author manuscript

Cell Rep. Author manuscript; available in PMC 2024 July 25.

Published in final edited form as:

Cell Rep. 2024 April 23; 43(4): 114006. doi:10.1016/j.celrep.2024.114006.

BRCA1 and 53BP1 Regulate Reprogramming Efficiency by Mediating DNA Repair Pathway Choice at Replication-associated Double-Strand Breaks

Daniela Georgieva[1,2,10], **Ning Wang**[1,2,10], **Angelo Taglialatela**[2,3], **Stepan Jerabek**[1,2,4], **Colleen R. Reczek**[3,9], **Pei Xin Lim**[5], **Julie Sung**[1], **Qian Du**[1], **Michiko Horiguchi**[2,8], **Maria Jasin**[4], **Alberto Ciccia**[2,3], **Richard Baer**[3,6], **Dieter Egli**[1,2,7,‡]

[1]Department of Pediatrics and Naomi Berrie Diabetes Center, Columbia University Irving Medical Center, New York, NY 10032, USA

[2]Columbia University Stem Cell Initiative, New York, NY 10032, USA

[3]Department of Genetics and Development, Herbert Irving Comprehensive Cancer Center, Columbia University Irving Medical Center, New York, NY 10032, USA.

[4]Institute of Organic Chemistry and Biochemistry of the Czech Academy of Sciences, Flemingovo namesti 542/2, 160 00 Praha 6, Czech Republic

[5]Developmental Biology Program, Memorial Sloan Kettering Cancer Center, New York, NY 10065, USA

[6]Department of Pathology & Cell Biology, Institute for Cancer Genetics, Columbia University Irving Medical Center, New York, NY 10032, USA.

[7]Department of Obstetrics and Gynecology, Columbia University Irving Medical Center, New York, NY 10032, USA

[8]current address: Department of Pharmaceutics, Faculty of Pharmaceutical Sciences, Tokyo University of Science in Yamaguchi, Sanyo-Onoda City, Yamaguchi 7550015, JAPAN

[9]current address: Northwestern University Feinberg School of Medicine, Chicago, IL 60611, USA

[10]equal contribution

SUMMARY

[‡]correspondence: de2220@cumc.columbia.edu.
lead contact: Dieter Egli

AUTHOR CONTRIBUTIONS

DG and DE designed the experiments. DG performed SFP and HDR and replication inhibitors in reprogramming. NW performed studies on the role of RGS and BRCA2, human iPS reprogramming, Western blot and contributions to other Figures. SJ and JS performed reprogramming experiments for manuscript revision, QD performed qPCR for p21. AT and AC provided mice and critical input. AT and MH performed DNA fiber analysis on *Brca1*$^{tr/+}$ and *ABC* immortalized MEFs. CRR generated mice with *Abraxas*^{S404A}, *Bach1*^{S994A} and *Ctip*^{S326A} mutant alleles. JS performed immunofluorescence. MJ and PXL generated the BRCA2^{SA} mouse embryonic fibroblasts and provided input on the study. DG analyzed data, created the figures and wrote the manuscript with contributions from NW, DE and RB, the latter also providing supervision.

DECLARATION OF INTERESTS

DG and DE have applied for a patent on interfering with 53BP1 during somatic cell reprogramming.

Reprogramming to pluripotency is associated with DNA damage and requires the functions of the BRCA1 tumor suppressor. Here, we leverage separation of function mutations in BRCA1/2 as well as the physical and/or genetic interactions between BRCA1 and its associated repair proteins to ascertain the relevance of homology-directed repair (HDR), stalled fork protection (SFP) and replication gap suppression (RGS) in somatic cell reprogramming. Surprisingly, loss of SFP and RGS is inconsequential for the transition to pluripotency. In contrast, cells deficient in HDR, but SFP and RGS proficient, reprogram with reduced efficiency. Conversely, the restoration of HDR function through inactivation of *53bp1* rescues reprogramming in *Brca1*-deficient cells, and *53bp1* mutants with elevated HDR show enhanced reprogramming in mouse and human cells. These results demonstrate that somatic cell reprogramming is especially dependent on repair of replication associated DSBs by the HDR activity of BRCA1 and BRCA2 and can be improved through 53BP1 loss.

INTRODUCTION

Somatic cells can be reprogrammed to pluripotency by ectopic expression of the four transcription factors OCT4, SOX2, KLF4 and cMYC (OSKM), which act as master regulators of the embryonic state[1]. The reprogrammed cell population, termed induced pluripotent stem (iPS) cells, is endowed with the capacity to proliferate indefinitely, and differentiate into any specialized cell type of the adult organism. These characteristics make iPS cells uniquely suitable for modelling human development and disease, drug discovery, and design of patient-specific cell replacement therapies. Nonetheless, overexpression of the reprogramming factors OSKM or OSK (without cMYC) results in increased levels of DNA damage, marked by the formation of γH2AX[2,3] and FANCD2 nuclear foci[4]. Of note, increased γH2AX and RPA foci are also seen during reprogramming by nuclear transfer, a process which does not entail the overexpression of transcription factors[5], implying that DNA damage is intrinsic to cell reprogramming. Since DNA damage during reprogramming has the potential for adverse genetic consequences compromising the utility of the resulting iPS cells, it is important to understand the origin and type of the damage, as well as the mechanisms of repair.

Determining the genetic requirements for DNA repair factors during reprogramming can point to the type of DNA damage that arises during this process. Of note, somatic cell reprogramming is severely compromised by mutations or knockdown of proteins implicated in homology-directed repair (HDR) of DNA double-strand breaks (DSBs), including Brca1 and Brca2[2], CtIP[6], Rad51[2], FancC and FancA[4], FancD2[7], and Atm[8]. In contrast, ablation of the tumor suppressors *p53*[9,10], *p21*[11] or *Rb*[12] results in more efficient iPS cell generation, suggesting that reprogramming is also governed by the molecular and cellular response to DNA damage.

Although BRCA1 has been implicated in many cellular processes, three aspects of its function are thought to be especially important for genome stability. First, BRCA1 is required for HDR, which repairs DSBs with high fidelity[13]. BRCA1 promotes the HDR pathway at multiple stages, including an early commitment step in which the decision is made to repair a DSB either by HDR or non-homologous end-joining (NHEJ). BRCA1

favors the choice of HDR over NHEJ by facilitating DNA end resection, a process that converts DSB ends into 3' ssDNA overhangs, which serve as key intermediates for HDR[14]. In addition, BRCA1 counters the activities of 53BP1, a protein which facilitates the recruitment of the shieldin complex to counteract DSB end resection and promote NHEJ[15,16]. Second, BRCA1 protects stalled DNA replication forks from nucleolytic degradation[17,18]. Interestingly, the HDR and stalled fork protection (SFP) activities of BRCA1 are genetically separable, and abrogation of SFP alone is sufficient to elicit chromosomal instability in response to replication stress, induced by treatment with hydroxyurea or mitomycin C[19]. Likewise, several other HDR factors have been implicated in the stability of stalled replication forks. For example, Rad51 promotes remodeling of stalled replication forks[20], CtIP protects stalled forks from nucleolytic degradation by DNA2[21]. Of note, BRCA2, like BRCA1, also protects stalled forks from degradation by MRE11[17,22]. Third, in addition to its involvement in HDR and SFP, BRCA1 has recently been shown to suppress the formation of ssDNA gaps arising during DNA replication in cancer cells[23,24], a function shared with BRCA2[25,26]. Since HDR, SFP and RGS all contribute to the genome maintenance functions of BRCA1, each individual process may be critical for BRCA1-mediated somatic cell reprogramming.

RESULTS

Reprogramming and homology-directed repair (HDR) are dependent on the interactions of BRCA1 with its BRCT phospho-ligands.

Reprogramming is severely impaired in mouse fibroblasts that are homozygous for either of two pathogenic *Brca1* lesions ($Brca1^{tr}$ and $Brca1^{S1598F}$)[2]. The $Brca1^{tr}$ allele encodes a C-terminally-truncated protein that lacks several critical BRCA1 domains, including its SQ cluster region, PALB2-binding sequence, and BRCT motif[27] (Fig.1A). In contrast, the protein product of $Brca1^{S1598F}$ harbors a single missense mutation that specifically disrupts the phosphate-binding cleft of the BRCT domain[28]. By virtue of its BRCT phospho-recognition domain, BRCA1 can interact with the phosphorylated isoforms of several DNA repair factors, including ABRAXAS, BACH1/BRIP1/FANCJ, and CtIP[29–31]. Since its interactions with each of these BRCT phospho-ligands are mutually exclusive, BRCA1 can form multiple distinct protein complexes *in vivo* (e.g., BRCA1 complexes A, B, and C) that may mediate different aspects of BRCA1 function.

To test whether the interaction of BRCA1 with one or more of its BRCT phospho-ligands is required for reprogramming, we examined mouse embryonic fibroblasts (MEFs) that are homozygous for serine-to-alanine substitutions in the critical phosphorylation sites of Abraxas (S404A), Bach1 (S994A) and/or Ctip (S326A). Previous studies of $Brca1^{S1598F/S1598F}$ cells have shown that BRCT phospho-recognition is required for both HDR[28] and SFP[19], as well as for reprogramming[2]. To ascertain whether these functions of Brca1 are dependent on its interactions with Abraxas, Bach1, and/or Ctip, we bred mice harboring the different combinations of homozygous Abraxas (*AA*), Bach1 (*BB*), and Ctip (*CC*) missense mutations and then evaluated HDR and SFP in MEFs and iPS cell lines from these mice. Although double-mutant *AABB*, *BBCC*, and *AACC* embryos appeared to develop normally relative to their wild-type littermates, the triple *AABBCC* mutants were smaller

on day E13.5 (Fig.1B). To assess HDR function in the different genotypes, we chose iPS cells as they can be grown in sufficient numbers for molecular analysis. Pluripotent stem cell lines were irradiated with 10Gy and examined for the formation of irradiation-induced foci of the Rad51 recombinase by immunofluorescent microscopy at 1.5-hour post treatment. Foci formation was significantly impaired in the triple-mutant *AABBCC* cells, while double-mutant *BBCC* and *AACC* cells showed modest, but not significant reduction (Fig.1C). To examine HDR competence, we conducted a CRISPR/Cas9-based DSB repair assay using cells that harbor a zsGreen-containing HDR template[32]. A dramatic reduction in HDR activity was observed in triple-mutant *AABBCC* cells, and the double-mutants *BBCC* and *AACC* also displayed a less severe HDR defect, as quantified using the dual allele edited cells, which form a distinct, fluorescently brighter, population (Fig.1D). To measure SFP function, immortalized MEFs derived from day E13.5 embryos were treated with hydroxyurea (HU) and the stability of stalled forks was assessed by analysis of IdU and CldU-stained DNA fibers, as described[19]. The rationale for the choice of immortalized MEFs was to allow for replicates as triple mutant embryos are rare, and primary MEFs were required for reprogramming studies. A marked reduction in the ratios of CldU/IdU track lengths, indicative of a profound SFP defect, was observed in triple-mutant *AABBCC* cells relative to wild-type cells (Fig.1E). In contrast, the track length ratios from each of the double-mutants were indistinguishable from those of wild-type cells (Fig.1E). As such, the triple-mutants, but not the double-mutants, reproduce the $SFP^{-}HDR^{-}$ phenotype observed in cells bearing tumor-associated *Brca1* mutations (*Brca1*$^{tr/tr}$ or *Brca1*$^{S1598F/S1598F}$ cells). Interestingly, *AACC* and *BBCC* double- mutants were compromised for HDR but retained normal SFP activity (Supplemental Table 1), permitting further dissection of BRCA1 functions required for reprogramming.

During reprogramming, we observed a modest, but significant, increase in γH2AX focus formation in the triple *AABBCC* mutants; increases were also seen in double-mutant (*AABB*, *BBCC* and *AACC*) MEFs, though not to significant levels (Fig.1F). While the yields of AP-positive colonies from double-mutant *BBCC* and *AACC* cells were lower than those of wild-type cells, the triple-mutant *AABBCC* displayed a marked reduction (~17-fold) in reprogramming efficiency, similar to the one reported for *Brca1*$^{tr/tr}$ and *Brca1*$^{S1598F/S1598F}$ MEFs (Fig.1G). Thus, the reductions in reprogramming efficiency (Fig.1G) paralleled those of HDR activity (Fig.1D), with modest decreases (2–3 fold for reprogramming and ~3-fold for HDR) in the *AACC* and *BBCC* mutants, which are SFP proficient, and a dramatic impairment (>10 fold for reprogramming and ~10- fold for HDR) in *AABBCC* cells, which are both HDR and SFP deficient. We also noted a reduction in both HDR and reprogramming in the *AABB* genotype, though the differences were less than 2-fold. Although the fold reductions in HDR and reprogramming within each mutant genotype are consistent, they are not identical, perhaps reflecting threshold effects or the contribution of other repair mechanisms during reprogramming.

Loss of stalled fork protection (SFP) does not affect reprogramming efficiency.

The above experiments implicate HDR as a primary determinant of reprogramming efficiency, but do not directly address the role of SFP. *In vivo*, BRCA1 exists as a heterodimer with BARD1, which also harbors a C-terminal BRCT domain[33]. The BRCT

domain of BARD1 binds in a phospho-specific manner to poly(ADP-ribose) (PAR)[34] and this interaction is required for recruitment of the BRCA1/BARD1 heterodimer to stalled replication forks and for BRCA1-mediated SFP activity[19] (Fig. 2A). Thus, by disrupting the interaction of Bard1 with PAR, *Bard1*^{K607A} and *Bard1*^{S563F} act as separation-of-function mutations that abrogate SFP without affecting HDR (Fig.2A and Supplementary Fig.1A); accordingly, *Bard1*$^{K607A/K607A}$ and *Bard1*$^{S563F/S563F}$ cells exhibit the HDR^{+}SFP^{-} phenotype[19] (Supplementary Table 1). In addition, although most biological functions attributed to *BRCA1*, including HDR, are unaffected in *BRCA1* heterozygotes, SFP is impaired in cells heterozygous for certain lesions in either *BRCA1*[18] or *BARD1*[19], including *Bard1*$^{K607A/+}$ and *Bard1*$^{S563F/+}$ MEFs.

HDR-competent SFP-deficient (i.e., HDR^{+} SFP^{-}) cells accumulate DNA breaks and chromosomal aberrations when exposed to replication stress[22 19 18]. To assess the consequences of SFP deficiency on DNA damage during reprogramming, we quantified the appearance of γH2AX and phospho-RPA(S33) foci on day 5 of reprogramming. This time point was chosen for analysis based on previous studies which showed elevated γH2AX focus formation in BRCA1 mutant cells compared to controls, from day 5 onward, persisting at least until day16 of reprogramming[2]. The numbers of γH2AX foci observed in *Brca1*$^{tr/+}$ and *Bard1*$^{K607A/K607A}$ cells were comparable to wild-type cells, indicating that SFP is not the primary mechanism preventing the accumulation of DNA damage during reprogramming (Fig.2B). The RPA/ssDNA filaments which form as a consequence of stalled fork processing are phosphorylated by the ATR kinase on Ser33 of the RPA2 polypeptide[35,36]. *Brca1*$^{tr/+}$ and *Bard1*$^{K607A/K607A}$ mutants showed no increase of phospho(S33)-RPA2 foci relative to wild-type cells during reprogramming (Fig.2C). Proliferation rates of *Brca1*$^{tr/+}$ and *Bard1*$^{K607A/K607A}$ cells on day 5 of reprogramming were indistinguishable from those of wild-type controls (Fig.2D), while the size and morphology of *Brca1*$^{tr/+}$ and *Bard1*$^{K607A/K607A}$ embryos at day E13.5 were also normal (Supplementary Fig.1B). Reprogramming efficiencies of all HDR^{+} SFP^{-} cells tested (*Brca1*$^{tr/+}$, *Bard1*$^{K607A/+}$, *Bard1*$^{K607A/K607A}$, *Bard1*$^{S563F/+}$ and *Bard1*$^{S563/S563F}$), as measured by the formation of alkaline phosphatase (AP) positive colonies, were indistinguishable from those of wild-type controls (Fig.2E and Supplementary Fig.1C). Thus, loss of Brca1-mediated SFP does not impair the efficiency of somatic cell reprogramming.

Restoring stalled fork protection in *Brca1*-mutant cells fails to improve reprogramming efficiency.

The SNF2-family of DNA translocases SMARCAL1, ZRANB3 and HLTF remodel newly stalled replication forks into reversed (‘chicken-foot’) intermediate structures that can facilitate fork restart (Fig.3A)[37]. Fork reversal generates a free DNA end that, although relatively stable in normal cells, can serve as a substrate for Mre11-dependent degradation in *BRCA1*-mutant cells[17]; by blocking fork reversal, Smarcal1 depletion can specifically rescue the SFP, but not the HDR function of *BRCA1* mutant cells[38]. Thus, while *Brca1*$^{tr/tr}$ cells display the HDR^{-} SFP^{-} phenotype, *Brca1*$^{tr/tr}$*Smarcal1*$^{-/-}$ cells are proficient for SFP and deficient for HDR (i.e., the HDR^{-}SFP^{+} phenotype, Supplementary Table 1).

To confirm that SFP is restored in *Brca1*$^{tr/tr}$*Smarcal1*$^{-/-}$ cells during somatic cell reprogramming, we performed DNA fiber analysis after exposure to hydroxyurea. In *Brca1*$^{tr/tr}$*Smarcal1*$^{-/-}$ cells, the IdU/CldU ratios are restored to wild-type controls (Fig.3B). The SFP proficiency of *Brca1*$^{tr/tr}$*Smarcal1*$^{-/-}$ cells was further established by DNA fiber analysis using the G-quadruplex stabilizing compound pyridostatin (PDS) (Supplementary Fig.2A), which stalls replication forks in G-rich regions of the genome[39], a physiologically relevant obstacle to DNA replication. As expected[38], *Brca1*$^{tr/tr}$*Smarcal1*$^{-/-}$ cells remained deficient for HDR (Fig.3C), confirming that they exhibit the HDR^{-} SFP^{+} phenotype.

Consistent with studies of human breast epithelial cells[38], DNA damage during reprogramming was significantly lower in *Brca1*$^{tr/tr}$*Smarcal1*$^{-/-}$ cells relative to *Brca1*$^{tr/tr}$ cells, as shown by reductions in both γH2AX (Fig.3D) and phospho-RPA(S33) (Fig.3E) focus formation. Nonetheless, loss of Smarcal1 (in *Brca1*$^{tr/tr}$*Smarcal1*$^{-/-}$ cells) failed to rescue either the proliferation defect (Fig.3F and Supplementary Fig.2B) or the elevated apoptosis (Fig.3G and Supplementary Fig.2C) of *Brca1*$^{tr/tr}$ fibroblasts during reprogramming. Moreover, *Brca1*$^{tr/tr}$ and *Brca1*$^{tr/tr}$*Smarcal1*$^{-/-}$ embryos were both significantly smaller on day E13.5 than either wild-type or *Smarcal1*$^{-/-}$ embryos (Supplementary Fig.2D). *Smarcal1*$^{-/-}$ null and heterozygous *Smarcal1*$^{-/+}$ MEFs reprogram with the efficiency of wild-type controls (Fig. 3H, Supplementary Fig.2E & F). In contrast, *Brca1*$^{tr/tr}$*Smarcal1*$^{-/-}$ cells, which have the HDR^{-} SFP^{+} phenotype, display a severe defect in iPSC generation (>11-fold reduction), equivalent to that of HDR^{-} SFP^{-} cells, such as *Brca1*$^{tr/tr}$ and *AABBCC* (Fig. 3H, Fig.1G). Thus, restoration of SFP is insufficient to rescue the reprogramming deficiency of *BRCA1*-mutant cells. Even though reprogramming efficiency in Brca1 tr/tr or *Brca1*$^{tr/tr}$*Smarcal1*$^{-/-}$ and other HDR-deficient mutants such as *AABBCC* is severely reduced, once reprogrammed, iPS cell lines could be established and propagated normally (Supplementary Table 2). Thus, despite their HDR impairment, these genotypes proved permissive of the pluripotent stem cell fate.

Ablation of *53bp1* restores efficient reprogramming in *Brca1*-mutant cells.

In normal cells, the decision to repair a DSB through either non-homologous end joining (NHEJ) or HDR is governed by the antagonistic relationship between 53BP1, which favors NHEJ by blocking resection of DSB ends and the BRCA1/BARD1 heterodimer, which favors HDR by displacing 53BP1[14,16,40] (Fig.4A). Consequently, inactivation of *53bp1* can restore the HDR function of *Brca1*-mutant cells by allowing for the resection and subsequent formation of ssDNA filaments at DSB ends[15,41].

We examined whether restoring HDR in *Brca1*-mutant cells would also rescue their reprogramming potential. Consistent with published literature, we confirmed that *Brca1*$^{tr/tr}$*53bp1*$^{-/-}$, but not *Brca1*$^{tr/tr}$, iPS cells are competent for HDR (Fig.4B). Previous studies have shown that the impact of 53BP1 loss on SFP varies between cell types[42]; here, we observed that the SFP defect of *Brca1*$^{tr/tr}$ cells was partially restored in the *53bp1*-null background of *Brca1*$^{tr/tr}$*53bp1*$^{-/-}$ MEFs (Fig.4C). Moreover, loss of 53bp1 in *Brca1*$^{tr/tr}$*53bp1*$^{-/-}$ cells reduced γH2AX and phospho-RPA(S33) focus formation relative to *Brca1*$^{tr/tr}$ (Fig.4D,E), while also restoring proliferation (Fig.4F and Supplementary Fig.3A) and reducing the levels of apoptosis during reprogramming (Fig.4G and Supplementary

Fig.3B). Importantly, the severe reprogramming defect of *Brca1*$^{tr/tr}$ MEFs was fully rescued by loss of *53bp1*, as shown by the restoration in AP+ colony numbers in *Brca1*$^{tr/tr}$*53bp1*$^{-/-}$ cells (Fig.4H and Supplementary Fig.3C, D). This rescue was also reflected in the increased numbers of Nanog positive cells (Fig.4I and Supplementary Fig.3E, F). Concordance between AP and nanog staining in the quantification of reprogramming efficiency was also confirmed in an earlier report[2]. Collectively, these findings indicate that efficient HDR promotes somatic cell reprogramming.

Loss of *53bp1* increases HDR activity and reprogramming efficiency in *Brca1*-proficient cells.

53BP1 regulates the balance between DSB repair pathways by promoting non-homologous end-joining (NHEJ) at the expense of HDR[15,16,40,41]. Accordingly, we observed that the HDR capacity of *53bp1*$^{-/-}$ cells is modestly (1.2-fold), but significantly, elevated relative to that of the wild-type controls (Fig.4B). Of note, the levels of proliferation (Fig.4F and Supplementary Fig.3A) and apoptosis (Fig.4G) were indistinguishable between *53bp1*$^{-/-}$ and wild-type cells, and no size differences were observed between *53bp1*$^{-/-}$ embryos and wild-type embryos at day E13.5 of development (Supplementary Fig.3G).

53bp1 loss was associated with a modest (up to 1.4 fold), but significant, increase in reprogramming efficiency as measured by AP+ colony numbers relative to both wild-type cells (Fig.4H) and SFP-deficient, but HDR-competent, *Brca1*$^{tr/+}$ mutants (Fig.4H and Supplementary Fig.3D). The enhanced reprogramming potential of the *53bp1*$^{-/-}$ genotype relative to wild type was further corroborated by immunofluorescence and flow cytometry data, which showed a 2-fold increase in the number of cells expressing the pluripotency maker Nanog (Fig.4I and Supplementary Fig.3E,F). Increased reprogramming efficiency was also demonstrated in human dermal fibroblasts. Downregulation of 53BP1 by RNAi during reprogramming (Supplementary Fig.3I,J) led to a ~2-fold increase in AP+ iPS colony formation (Fig.4J and Supplementary Fig.3J, K).

To investigate how 53BP1 affects iPS cell generation, we examined 53bp1 focus formation in response to DNA damage during reprogramming. As expected, *Brca1*$^{tr/tr}$ cells, which are defective for both HDR and SFP, displayed elevated levels of 53bp1 foci relative to wild-type cells (Fig.5A). In contrast, all HDR^{+} SFP^{-} cells, including *Brca1*$^{tr/+}$, *Bard1*$^{K607A/K607A}$ and *Bard1*$^{S563F/S563F}$ cells, formed 53bp1 foci at levels similar to those observed in the wild-type (Fig.5A). Notably, 53bp1 focus formation in *Brca1*$^{tr/tr}$*Smarcal1*$^{-/-}$ cells, which display the HDR^{-} SFP^{+} phenotype, occurred at elevated levels, similar to those of *Brca1*$^{tr/tr}$ cells, demonstrating that restoration of SFP activity does not reduce 53bp1 focus formation (Fig.5A). These results reveal a negative correlation between iPS cell generation and 53bp1 assembly at sites of DSB repair.

In addition to its role in DSB repair by NHEJ, 53BP1 has a separate function in the stimulation of p53-dependent transcription of the p21 cell cycle inhibitor and of the pro-apoptotic proteins BAX and PUMA/BBC3 in human metastatic adenocarcinoma[43]. Another study showed normal stabilization of p53 and IR-induced upregulation of p21 in *53bp1*$^{-/-}$ mouse thymocytes[44], demonstrating that the impact of 53bp1 on p53 function may vary with cell type. Nonetheless, since downregulation of either p53 or p21 has been shown

to improve iPS cell generation[11], we examined expression of p21 during reprogramming. We detected no changes in proliferation (Fig.4F and Supplementary Fig.3A) or apoptosis (Fig.4G) of *53bp1*$^{-/-}$ cells relative to wild-type controls and detected no difference in p21 expression levels in primary MEFs (Supplementary Fig.3L, M) or during reprogramming (Fig.5B). Therefore, the enhanced reprogramming efficiency of *53bp1*$^{-/-}$ cells is not due to compromised expression of the p53 transcriptional target p21.

Replication-associated DSBs limit somatic cell reprogramming.

The genetic requirements for DSB repair during iPS cell generation point to the type of DNA damage that impairs reprogramming. DSBs arising during replication at stalled and collapsed forks are typically one-ended[45–47], and in normal cells these breaks are preferentially repaired by HDR[40,48]. In contrast, two-ended DSBs can be induced by exogenous sources, such as ionizing irradiation or Cas9 cleavage, or occur endogenously due to oxidative stress or the programmed genetic rearrangements arising during lymphocytes development. While two-ended DSBs are productively repaired by either NHEJ or HDR, one-ended DSBs from replication intermediates are not suitable for NHEJ and their mis-repair can yield aberrant, potentially toxic, chromosomal rearrangements.

To determine which types of DSBs affect the efficiency of iPS cell generation, we treated reprogramming MEFs with the DNA polymerase inhibitor aphidicolin, which can induce the formation of replication-associated DSBs due to replication fork slowing[48]. Treatment of uninfected wild-type fibroblasts with a low concentration of aphidicolin resulted in elevated numbers of 53bp1 nuclear foci (Fig.5C). Wild-type cells exposed to low aphidicolin throughout an 8-day period during reprogramming show 2-fold reduction in iPS cell colony formation (Fig.5D). The inhibitory effect of aphidicolin on reprogramming was more pronounced in *Brca1*$^{tr/tr}$ cells (Fig.5E). (A higher bar in Figures 5E–H corresponds to greater sensitivity and lower reprogramming efficiency relative to untreated cells.) *53bp1*$^{-/-}$ mutant MEFs were less sensitive to aphidicolin than wild-type cells, and *Brca1*$^{tr/tr}$*53bp1*$^{-/-}$ cells were less sensitive to aphidicolin than *Brca1*$^{tr/tr}$ cells (Fig.5E). Since low concentrations of aphidicolin increases chromosome breakage[49], these results suggest that efficient reprogramming is dependent on the efficient repair of replication-induced lesions by HDR.

To further explore the impact of replication-associated DSBs on cell reprogramming, we also tested topotecan, a topoisomerase I inhibitor. At low concentrations, topotecan generates single-strand nicks that can be converted to one-ended DSBs during DNA replication[50]. While topotecan treatment resulted in a small reduction in reprogramming efficiency of wild-type cells (Fig.5F), it dramatically reduced reprogramming efficiency of HDR-deficient *Brca1*$^{tr/tr}$ MEFs (Fig.5F). This phenotype was partially rescued in HDR-proficient *Brca1*$^{tr/tr}$*53bp1*$^{-/-}$ cells (Fig.5F). Furthermore, loss of 53bp1 in wild-type cells also decreased their sensitivity to topotecan exposure during reprogramming (Fig.5F). These results indicate that HDR-mediated repair of replication-associated DSBs is limiting for efficient iPS cell generation.

It was previously reported that Parp1 is required for OSKM-mediated reprogramming in MEFs[51] and that Parp1 inhibition results in the accumulation of replication-associated

DSBs[52,53]. To understand the consequences of Parp1 inhibition on reprogramming, we exposed different genotypes to Olaparib. Although a low concentration of Olaparib (50nM) did not affect the reprogramming efficiency of wild-type controls (Fig. 5G, Supplementary Fig.4C), it reduced the reprogramming of HDR-deficient *Brca1*-mutant MEFs (Fig.5G). As with aphidicolin and topotecan, the reduced reprogramming of *Brca1*-mutant cells was fully restored on a *53bp1*-null background (Fig.5G). Although this result is consistent with the genetic requirements for the repair of replication-associated DSBs, it should be noted that PARP inhibition also increases the incidence of ssDNA gaps[54, 55]. Since BRCA1-deficient cells have elevated frequencies of ssDNA gaps in both unstressed conditions and upon exposure to DNA damaging agents[23,24], the impact of ssDNA gap formation on reprogramming is addressed below.

To evaluate the impact of two-ended DSBs on iPS cell formation, we administered a single dose (1Gy, 3Gy or 6Gy) of ionizing irradiation (IR) one day after doxycycline induction of the OSKM reprogramming factors. Although IR treatment reduced reprogramming efficiency in all genotypes types tested, $53bp1^{-/-}$ cells were modestly, but significantly more sensitive than wild type cells at all levels of IR exposure (Fig.5H, Supplementary Fig.4A,B). This result contrasts with the lower sensitivity of $53bp1^{-/-}$ fibroblasts to treatment with aphidicolin (Fig. 5F) or topotecan (Fig. 5E) during reprogramming. In $Brca1^{tr/tr}$ cells, IR at all doses elicited a marked reduction in reprogramming potential (Fig.5H and Supplementary Fig.4A,B). However, in contrast to aphidicolin or topotecan exposure, the reprogramming efficiency of IR-treated MEFs was only partially restored by loss of 53bp1 in $Brca1^{tr/tr}$ cells ($Brca1^{tr/tr}$vs. $Brca1^{tr/tr}53bp1^{-/-}$ genotypes) (Fig.5H, Supplementary Fig.4A,B). These results indicate that increasing the load of two-ended DSBs during reprogramming impedes iPS cell generation in 53bp1-null cells, presumably reflecting the role of 53bp1 in NHEJ repair of two-ended DSBs[56]. Collectively, the genetic requirements for the repair of replication-associated DSBs matches the genetic requirements for efficient reprogramming, while repair of two-ended DSBs do not.

HDR of DSBs, rather than ssDNA gap suppression, is the primary function of BRCA1 in reprogramming.

To examine the role replication gap suppression (RGS) in somatic cell reprogramming, we examined ssDNA gap formation using the S1 nuclease assay. S1 nuclease specifically cleaves ssDNA, and thereby shortens IdU/CldU-labelled replication tracks with ssDNA gaps[57] (Fig.6A). Cells homozygous for a $Brca1^{tr/tr}$ displayed a significant increase in ssDNA gap formation both in reprogrammed iPS cell lines (Fig.6B) and in MEFs undergoing reprogramming (Supplementary Fig.4D,E).

To ascertain whether reprogramming is dependent on HDR, RGS, or both, we examined ssDNA gap formation in *AABBCC* cells, which display a profound defect in reprogramming (Fig.1G), comparable to pathogenic *Brca1* mutants, such as $Brca1^{tr/tr}$ and $Brca1^{S1598F/S1598F}$ cells[2]. In contrast to the increased ssDNA gap formation observed in $Brca1^{tr/tr}$ and $Brca1^{S1598F/S1598F}$ MEFs, ssDNA gaps are not elevated in *AABBCC* cells relative to wild-type controls (Fig.6C and Supplementary Fig.4D,E). Likewise, ssDNA gaps were not detected in the double combination mutants (*AACC* and *BBCC)* (Fig.6C and Supplementary

Fig.4D,E) which displayed modest, but significant reductions in both reprogramming potential (Fig.1G) and HDR (Fig.1D). In our experiments, the difference in spontaneous ssDNA gap formation between the *Brca1*$^{tr/tr}$ and *AABBCC* genotypes implies that deficiency in HDR, and not RGS, is primarily responsible for the impaired reprogramming capacity of *Brca1*-mutant cells.

To further examine the role of RGS, we also examined the impact of two well-defined Brca2 mutations on iPS cell formation: *Brca2*^{S3214A} (referred to as *Brca2*^{SA}), which encodes a serine-to-alanine substitution of amino acid 3214, and *Brca2*$^{\Delta 27}$, which encodes a C-terminally truncated Brca2 polypeptide lacking residues 3140–3328, including S3214. Heterozygous and homozygous mutants of *Brca2*$^{SA/SA}$ mutants are deficient for RGS and SFP, but retain HDR function[58]. Here, we confirm that RGS in *Brca2*$^{SA/SA}$ cells is also impaired during reprogramming (Fig.6D). Despite RGS deficiency, reprogramming of *Brca2*$^{SA/SA}$ and *Brca2*$^{+/SA}$ cells is not impaired (Fig. 6E, Supplementary Fig.4F). Furthermore, heterozygous *Brca2*$^{\Delta 27/+}$ cells deficient for RGS and SFP also reprogrammed with the efficiency of wild type cells (Fig.6F), while homozygous *Brca2*$^{\Delta 27/\Delta 27}$ cells deficient for all three functions HDR, RGS and SFP[59] failed to reprogram.

DISCUSSION

The mechanisms safeguarding cellular identity are an important question in developmental biology. Previous reprogramming studies have identified histone and DNA methylation, chromatin assembly factors, and posttranslational modifications as important determinants of iPS cell formation[60]. While most studies have focused on barriers to changes in gene expression, there is mounting evidence that the DNA damage response and cell cycle checkpoints play a key role in safeguarding the somatic state. Somatic cell reprogramming results in increased DNA damage, as manifested by elevated γH2AX nuclear foci[2,3,5]. In the context of somatic cell nuclear transfer, DNA damage is acquired during DNA replication, starting from the first cell cycle[5]. During iPS reprogramming, γH2AX foci are elevated no later than 4 days after reprogramming factor induction, and remain elevated for at least 2 weeks[2,3]. Thus, DNA damage and repair throughout the reprogramming process can impact the formation and quality of the resulting iPS cells. Notably, BRCA1 mutant iPS cell lines can be established at a reduced rate, suggesting that the requirement for BRCA1 is greater during the reprogramming process than in stable somatic and iPS cell cultures.

Pathogenic *BRCA1* lesions tested prior to this study each abrogate all three of the primary mechanisms by which BRCA1 preserves genome integrity: homology-directed repair (HDR)[13], stalled replication fork protection (SFP)[17] and replication gap suppression (RGS)[23,24]. Here, we used separation-of-function mutations and genetic rescue experiments to ascertain the dependence of somatic cell reprogramming on each of these BRCA1 functions.

To specifically interrogate the relevance of SFP and RGS in iPS cell generation, we examined cells bearing different genotypes that abrogate SFP while leaving HDR intact, including heterozygous *Brca1*$^{tr/+}$ mutants and cells that are either homozygous or heterozygous for the *Bard1* separation-of-function mutations *Bard1*^{K607A} or *Bard1*^{S563F}.

Although these cells all display an HDR^+ SFP^- phenotype, each underwent reprogramming at efficiencies comparable to those of wild-type controls. Conversely, while loss of the DNA translocase SMARCAL1 restored SFP but not HDR function in *Brca1* mutant cells, reprogramming remained compromised. Together, these results rule out a major requirement for SFP in somatic cell reprogramming. Notably, $BRCA2^{SA}$ mutant cells, which are deficient in RGS and SFP[59], display normal reprogramming potential, providing support for the notion that neither RGS and SFP are not limiting for reprogramming. By contrast, in all settings tested, reprogramming efficiency was highly sensitive to HDR efficiency.

Although somatic cell reprogramming is accompanied by elevated formation of DSBs[2–5], the nature and origin of these breaks remains poorly understood. A distinction between one-ended and two-ended DSBs can be made based on their mechanism of formation and the genetic requirements for their repair. Two-ended DSBs can be repaired productively by either NHEJ or HDR. One-ended DSBs, which are generated primarily during S-phase through processing of collapsed replication forks and through forks encountering ssDNA breaks[45,46,61], are preferentially repaired by HDR. In this context, 53BP1 mutations, by favoring HDR over NHEJ repair, would be expected to enhance iPS formation. Indeed, we observed that reprogramming of *53bp1*$^{-/-}$ fibroblasts was less sensitive to inducers of one-ended DSBs than wild-type cells during reprogramming, but was more vulnerable to two-ended DSBs generated by IR. This is consistent with the sensitivity of *53bp1*$^{-/-}$ mice and embryonic cells to IR[56]. These results collectively indicate that the limiting factor for reprogramming to pluripotency is a replication associated DSB, which requires repair by HDR.

A recent study has shown that among these three functions (HDR, SFP and RGS) of the BRCA2 tumor suppressor, HDR is the most significant contributor to genome stability and chemotherapeutic sensitivity in the context of cancer[59]. Likewise, among these separable BRCA1/2 functions, we show here that HDR efficiency is also the most significant determinant of efficient iPS reprogramming. Previous studies have pointed out additional genetic parallels between reprogramming and tumorigenesis[9,62], showing that reprogramming is facilitated by the loss of tumor suppressors which orchestrate the response to unrepaired DNA damage, such as p53[9], p21[11] or Rb[12]. As for tumor formation, replication-associated DNA damage is a barrier in the transition from somatic cell to pluripotent state[3,5,63]. In this study, we demonstrate that DSBs formed during DNA replication can suppress somatic cell reprogramming and that their proper resolution by the HDR pathway is essential for efficient iPS cell generation. In the absence of HDR, unresolved DNA repair intermediates can persist through G2, into mitosis and the next G1[64], during which the retained damage suppresses further cell cycle progression through activation of p53, p21 and Rb[65,66]. Interestingly, p21 and Rb both have inhibitory consequences on OSKM-mediated transcriptional reprogramming, repressing expression of pluripotency factors and promoting maintenance of repressive histone marks[12]. Therefore, by affecting both cell cycle progression and transcriptional reprogramming, an unrepaired replication-associated DSB inhibits iPS formation. While a mutation of p53, p21 or Rb might improve reprogramming efficiency by decreasing the response to DNA damage, 53BP1 knockout increases reprogramming efficiency by increasing HDR, the repair pathway

most relevant to reprogramming. Inhibiting 53BP1 might thus be a safer way to increase reprogramming efficiency than checkpoint interference.

Reduced reprogramming efficiency is one consequence of genome instability, but *de novo* mutations and alterations in chromatin modifications or architecture may be another product of DNA replication stress. Replication stress during reprogramming contributes to copy number changes[67], compromising their utility in research and therapy, and has indeed adversely affected an autologous cell therapy trial[68]. Future studies should thus aim to determine the importance of different repair pathways in the quality of the resulting iPS cells, including their genetic integrity and developmental potential.

LIMITATIONS OF STUDY

The study does not currently determine the impact of different DNA repair mechanisms on the quality of the resulting iPS cell lines. The study also does not distinguish the temporal requirements of different repair pathways during somatic cell reprogramming. Furthermore, the conclusion that the one-ended DSB is the DNA lesion primarily responsible for affecting reprogramming efficiency is inferred from the genetic requirements of efficient reprogramming, and is not directly determined by methods that can visualize these breaks directly.

STAR Methods

RESOURCE AVAILABILITY

Further information and requests for resources and reagents should be directed to and will be fulfilled by the Lead Contact, Dieter Egli (de2220@cumc.columbia.edu)

Materials Availability—Requests for iPSC lines or mice should be addressed to Dieter Egli. Columbia University requires the completion of an MTA for the distribution of materials.

Data and Code Availability

- Data reported in this paper will be shared by the lead contact upon request.
- This paper does not report original code
- Any additional information required to reanalyze the data reported in this paper is available from the lead contact upon request.

EXPERIMENTAL MODEL AND STUDY PARTICIPANT DETAILS

Animals—All mouse experiments performed in this study are in compliance with ethical regulations regarding the use of research animals and were approved by the Columbia University IACUC. Animals are housed in a barrier facility in individually ventilated cages.

To generate Bard1 mutants, heterozygous *Bard1*$^{K607A/+}$ and *Bard1*$^{S563F/+}$ females on a C57BL/6J background[19] were bred to males of the same genotypes at ages 10–50 weeks of age. The *Brca1/Smarcal1* genotype panel was created from intercrosses between

Brca1$^{tr/+}$*Smarcal1*$^{+/-}$ animals of mixed C57BL/6J and 129Sv background. The *Brca1*$^{tr/+}$ allele is described in[27]. Mice mutant for *Smarcal1* were obtained from the International Mouse Phenotyping Consortium (IMPC). The *Brca1/53bp1* genotype panel was generated from intercrosses between *Brca1*$^{tr/+}$*53bp1*$^{+/-}$ males and females on a mixed C57BL/6J and 129Sv background. The *Abraxas/Bach/Ctip* genotype panel was also generated on a mixed background (C57BL/6J and 129Sv) by crossing homozygous *Ctip*$^{S326A/S326A}$ mice[69] (designated here as "*CC*" mice and available from Jackson under strain #036502) with double homozygous *Abraxas*$^{S404A/S404A}$*Bach1*$^{S994A/S994A}$ mice (kindly provided by Dr. Thomas Ludwig, Columbia University, and designated here as "*AABB*" mice). The F1 triple heterozygous ("*A+B+C+*") progeny was then intercrossed to obtain the different combinations of double homozygous mutants. To generate triple homozygous *AABBCC* mice, the F2 *A+BBCC* males were crossed to F2 *A+BBCC* or *A+BBC+* females. From the *A+BBCC* × *A+BBCC* crosses, 1 of 9 embryos was triple homozygous *AABBCC* (expected Mendelian ratio is 1/4). One additional *AABBCC* embryo was obtained from triple heterozygous intercrosses (*A+B+C+* × *A+B+C+*) that produced 69 embryos (expected Mendelian ratio is 1/64). BRCA2^{S3214A} (BRCA2^{SA}) mice and their characterization of SFP and RGS were described recently[59].

Mouse Embryonic Fibroblasts—To derive fibroblasts for reprogramming, we harvested E13.5 mouse embryos from the above described crosses and processed them as in[70] with minor modifications. The cells from a single embryo were then plated in one 10cm dish and grown in MEF media, consisting of DMEM HG (Thermo Fisher Scientific #10569010), supplemented with 10% FBS (Atlanta Biologicals #S11150), Glutamax (Thermo Fisher Scientific #35050079) and PenStrep (Thermo Fisher Scientific 15140163). Cells were split once to P1 and frozen down for reprogramming experiments. The sequences of all genotyping primers are provided in Supplementary Table 3.

Mouse iPSC lines—A list of all mouse iPSCs cell lines and their genotypes is provided in Supplementary Table 2. Methods for growing mouse iPSCs are provided in the Methods details.

Human Cell Lines—Somatic human cells from an adult male (ID#1023) were used, available from a public cell repository (https://www.eglilab.com/cell-line-repository). All research with human cells was approved by the Columbia University Embryonic Stem Cell Research Oversight Committee and by the IRB.

METHOD DETAILS

Virus preparation and infection—This study used a doxycycline inducible lentiviral system, consisting of Tet-O-FUW-OSKM (Addgene #20321) and FUW-M2rtTA (Addgene # 20342). Lentivirus was prepared in 293T cells by transfection of plasmids with Jetprime transfection reagent (VWR #89129–922) as outlined in the manufacturer's instructions. Briefly, Tet-O-FUW vectors were transfected together with the envelope and packaging plasmids from Didier Trono pMD2VSVG (Addgene #12259) and psPax2 (Addgene # 12260) into 293T cells plated on collagen-coated dishes. Fresh antibiotic-free media DMEM HG (Thermo Fisher Scientific #10569010), supplemented with 15% FBS (Atlanta

Biologicals #S11150) and Glutamax (Thermo Fisher Scientific #35050079) was provided 16 to 20h post transfection. Viral supernatant was collected on each of the following two days and kept at 4C for up to 4 days. Prior to infection, titer from the two collection days was pooled and filtered through a 40μm cell strainer (Fisher Scientific #08-771-1).

For infection, P1 mouse embryonic fibroblasts (MEFs) were thawed and plated at 1×10^6 cells per 10cm dish on the previous day. Infection proceeded in two rounds with 8h to 9h in between. Briefly, cells were incubated with an OSKM/rtta virus mix (1:1), supplemented with 8ug/ml protamine sulfate (Fisher Scientific #0219472905). The infection mix was removed on the following day and cells were left to recover in fresh MEF media (DMEM HG Thermo Fisher Scientific #10569010 with 10% FBS Atlanta Biologicals #S11150, Glutamax Thermo Fisher Scientific #35050079 and PenStrep Thermo Fisher Scientific 15140163).

Reprogramming—Two days after infection, cells were re-plated on gelatin-coated dishes for transduction efficiency assessment on day 3, molecular analyses on day 5, colony picking on day 16 and alkaline phosphatase (AP) staining on day 20. In each experiment, infected fibroblasts from the different genotypes were re-plated at multiple densities to allow for optimal reprogramming efficiency. For wild-type cells, 100–300cells/mm^2 (20–60K per well of a 24w dish) routinely generated high numbers of iPS cell clones. Besides for wild type, 20,000–60,000 per well of a 24w dish was also optimal for the *Bard1* point mutants, $Brca1^{tr/+}$ (and all combination mutations with Smarcal1 or 53bp1), $Brca1^{tr/tr}53bp1^{-/-}$ as well as the heterozygous or homozygous *Smarcal1* and *53bp1* single mutants. The 3 genotypes- $Brca1^{tr/tr}$; $Brca1^{tr/tr}Smarcal1^{+/-}$ and $Brca1^{tr/tr}Smarcal1^{-/-}$ were plated at 600–800cells/mm^2 (120,000–160,000 per well of a 24w dish) to obtain any reprogramming; we observed no iPS clones at the densities selected for wild type for these genotypes. The $Brca1^{tr/tr}53bp1^{+/-}$ genotype was re-plated at 450cells/mm^2 (90K/well of a 24w dish). These seeding densities were used to calculate reprogramming efficiency of each genotype. Reprogramming experiments involving $BRCA2^{SA}$ and $BRCA2^{\Delta27}$ genotypes and controls used blinding to sample identity and cells of all genotypes were seeded at 40K cells per well.

The OSKM reprogramming factors were induced with 1ug/ml doxycycline (Sigma # D9891) in mouse embryonic stem (mES) cell media, consisting of Knockout DMEM (Life Technologies #10829–018), supplemented with 15% Knockout Serum Replacement (Life Technologies #10828–028), Glutamax (Thermo Fisher Scientific #35050079), MEM NEAA (Life Technologies #11140050), PenStrep (Thermo Fisher Scientific 15140163), 2-mercaptoetahnol (Life Technologies #21985–023) and 10ng/ul LIF (eBioscience #34-8521-82). Transduction efficiency was determined on reprogramming day 3 by staining for Sox2 (Stemgent #09–0024) and used in the calculation of reprograming efficiency.

mES media was also used for routine culture of iPS cell lines. Mouse iPSCs were maintained in feeder-free condition on 0.1% gelatin-coated (Millipore #ES-006-B) tissue culture plates in standard miPSCs medium, consisting of Knockout DMEM (Life Technologies #10829–018), supplemented with 15% ESC grade FBS (Atlanta Biologicals #S11150), Glutamax (Thermo Fisher Scientific #35050079), MEM NEAA (Life Technologies #11140050), PenStrep (Thermo Fisher Scientific 15140163), 2-

mercaptoetahnol (Life Technologies #21985–023) and 10 ng/uL LIF (eBioscience #34-8521-82). Splitting was performed with TrypLE (Life Technologies).

The reprogramming experiments with drug treatment used aphidicolin (Sigma #A0781) at 0.2μM, topotecan (Sigma #T2705) at 10nM or olaparib at 50nM (Selleckchem #S1060) for 8 days during reprogramming. Alternatively, for the induction of two-ended DSBs, cells were subjected to a single dose of 3Gy or 6Gy IR 1day post doxycycline-mediated OSKM factor induction. Cells were fixed on reprogramming day 18–20 and stained for alkaline phosphatase with the Vector Red detection kit (Vector Laboratories #SK-5100). Reprogramming efficiency was determined by considering the number of AP-positive colonies per number of infected cells, determined by Sox2 staining at the optimal plating density for each genotype. The sensitivity score to drugs was obtained by calculating the ratio of treated wild type (normalized to untreated wild type) to treated mutant (normalized to untreated mutant). A high score represents greater sensitivity and lower reprogramming.

The reprogramming experiments with human cells used ID1023 dermal fibroblasts, from an adult male. To downregulate 53BP1, 1023 fibroblasts were transfected with 53BP1-siRNA (Sigma, SASI_Hs01_00024577) in Jetprime transfection reagent (VWR #89129–922), according to the manufacturer's instructions. Cells were harvested 48h post siRNA transfection for qPCR and WB. Three days after siRNA transfection, cells were transduced with sendai virus reprogramming vectors (hKOS, hc-Myc and hKlf4) from the CytoTune-iPS 2.0 Sendai Reprogramming Kit (Thermo Fisher Scientific #A16517) with a MOI as outlined in the manufacture's protocol. On day 7 after sendai virus transduction, cells were re-plated on geltrex-coated 24-well dishes and from day 8 onward, were cultured in Stemflex medium (Gibco #A3349401).

RT-qPCR, Western Blot and Immunofluorescence—Total RNA from human fibroblasts (ID#1023) was extracted with the RNeasy Mini Kit (Qiagen #74104) according to the manufacturer's protocol. 1 ug of RNA was reverse-transcribed using the iScript™ cDNA Synthesis Kit (Bio-RAD #1708891). The RT-qPCR reactions were prepared in triplicates with the AzuraView™ GreenFast qPCR Blue Mix (Azura Genomics #AZ-2305) and the products were detected in a CFX96 real-time PCR system (Bio-Rad, Hercules, CA, USA). The reaction condition were: 95°C for 2min, and 40 cycles of 95°C for 5s and 60°C for 30 s. The relative expression level of genes was normalized to that of GAPDH and calculated using 2–ΔΔCt method. The sequences of primers used in this study were:

53BP1 Forward: 5'-ATGGACCCTACTGGAAGTCAG

53BP1 Reverse: 5'-TTTCTTTGTGCGTCTGGAGATT

GAPD Forward: 5'-GGAGCGAGATCCCTCCAAAAT

GAPDH Reverse: 5'-GGCTGTTGTCATACTTCTCATGG

P21 Forward: 5'-GCCTTAGCCCTCACTCTGTG

P21 Reverse: 5'-AGCTGGCCTTAGAGGTGACA

Beta actin Forward: 5'-GGCTGTATTCCCCTCCATCG

Beta actin Reverse: 5'-CCAGTTGGTAACAATGCCATGT

For p21 detection, protein was harvested from wild-type and *53bp1*-mutant uninfected MEFs as well as MEFs of the same genotypes on reprogramming day 5. Lysis was performed in RIPA buffer and proteins of interest were detected with the following antibodies: rabbit αp21 (Abcam #ab188224) and rabbit α-alpha tubulin (Abcam #ab4074). 53BP1 was detected in human dermal fibroblasts 48h post siRNA transfection with mouse α53BP1 (BD Biosciences #BD612522).

Detection of phospho-H2AX(S139), i.e. γH2AX, phospho-RPA(S33) and 53bp1 was performed by immunofluorescence on reprogramming day 5 with the following antibodies: mouse αphospho-histone H2A.X-Ser139 (Millipore #05–636), rabbit αphospho-RPA2Ser33 (Invitrogen #PA5–39809), rabbit α53BP1 H-300 (Santa Cruz #22760, 1:50 dilution). Quality controls: the rabbit α-phospho-RPA2Ser33 does not react to S33A mutant[71]. The antibody αphospho-histone H2A.X-Ser139 does not react to S139A-mutant H2AX[72]. 53BP1 foci co-localized with γH2AX (Fig. S4G).

The numbers of phospho-H2AX(S139) and phospho-RPA(S33) foci were counted in an automated manner by scanning stained slides with the Metafer4-Metacyte system and applying the same counting algorithm to all samples. Only large, unmistakable foci were considered and small specs of staining were excluded to avoid false positives. 53BP1 foci were counted with the Olympus cellSens software. For detection of Rad51, iPS cell lines were irradiated with 10Gy and stained with Rad51 (Ab-1) rabbit pAb (Millipore # PC130) 1.5h post IR. Quality control: this antibody has previously been shown to detect ATR dependent Rad51 foci formation[73]. Foci numbers were determined by using the counting and analysis function of the Olympus cellSens software. Nanog expression was evaluated on reprogramming day 20 with rabbit αNanog (Reprocell #RCAB001P2P) antibody. TRA-1–60 was detected in human cells with Alexa Fluor 488 conjugated mouse αhuman TRA-1–60 (BD Biosciences #BD560173).

DNA fiber analysis—DNA fiber analysis on *Brca1*, *Smarcal1* and *53bp1* combination mutants during reprogramming was carried out as described in Terret et al. 2009[74]. Briefly, fibroblasts of different genotypes were incubated on reprogramming day 5 with 25μM CldU for 30min, washed 3 times with warm PBS and incubated with 125μM IdU for another 30min. Fork stalling was induced by a 5h-long treatment with 2mM hydroxyurea (HU). In an alternative fiber assay, fork stalling was induced by treatment with 2μM pyridostatin (PDS) during the 30min incubation with 125μM IdU.

Fiber experiments with the *ABC* genotype collection and the $Brca1^{tr/+}$ genotype were performed on uninfected immortalized MEFs. Cells from the *ABC* genotypes were incubated with 200μM IdU for 20min, washed three times with PBS and then incubated with 100μM CldU for 20min. Fork stalling was induced by treatment with 2mM HU for 1.5h. In some conditions, 50μM mirin was added during the pulse labelling steps with IdU and CldU as well as during incubation with HU. Immortalized MEFs from the $Brca1^{tr/+}$

genotype and controls were incubated with 50μM CldU for 20min, followed by 3 washes with PBS and 250μM IdU for 20min. Fork stalling was induced by treatment with 2mM HU for 1.5h.

Fibers were stretched on slides and stained with BrdU/CldU (Biorad # OBT0030) and BrdU/IdU (BD # 347580) antibodies. Imaging was performed with a 100x objective on an Olympus microscope and fiber length was measured with Olympus cellSens imaging and analysis software.

HDR Assay—The HDR competence of the different genotypes was evaluated in mouse induced pluripotent stem (iPS) cells with a CRISPR/Cas9-based assay where a zsGReen repair template is targeted to the Hsp90 genomic locus. This strategy has been described in detail by Mateos-Gomez et al.[32]. In short, 200–300×10^3 exponentially growing iPS cells were transfected with 200ng Cas9-puromycin vector and 800ng zsGreen repair template with Jetprime transfection reagent (VWR #89129–922) as outlined in the manufacturer's instructions. Media was changed ~20h post transfection for 24h. To enrich for Cas9-transfected cells, the plates were treated with 1ug/ml puromycin (Thermo Fisher #A11138–03) for ~20h. Flow cytometry for zsGreen was performed on the 3rd day of recovery form puromycin selection. To exclude potentially non-transfected cells, the efficiency of single versus dual allele targeting was compared.

Proliferation and apoptosis—To evaluate proliferation, infected fibroblasts on reprogramming day 2 were incubated with 5μM Cell Trace CSFE proliferation dye (Thermo Fisher # C34554) for 20min at 37C as outlined in the manufacturer's protocol. Cells were then changed to fresh mouse ES cell media, composed of Knockout DMEM (Life Technologies #10829–018), 15% Knockout Serum Replacement (Life Technologies #10828–028), Glutamax (Thermo Fisher Scientific #35050079), MEM NEAA (Life Technologies #11140050), PenStrep (Thermo Fisher Scientific 15140163), 2-mercaptoetahnol (Life Technologies #21985–023) and 10ng/ul LIF (eBioscience #34-8521-82), supplemented with 1ug/ml doxycycline (Sigma # D9891). Three days post incubation with CSFE (reprogramming day 5) cells were harvested for flow cytometry.

For apoptosis analysis, cells were collected on reprogramming day 5 and stained without fixation with the Annexin V-FITC apoptosis detection kit (Sigma # APOAF-20TST) according to protocols provided by the manufacturer. The numbers of early and late apoptotic cells were determined by flow cytometry for Annexin V-FITC and propidium iodide (PI). Early apoptosis is marked by Annexin V staining only, while late apoptotic cells stain for both Annexin V and PI.

Nanog Detection—Cells were harvested on reprogramming day 20 and fixed in 4% paraformaldehyde for 15 min at RT. Staining was performed by standard protocol with rabbit αNanog primary AB (Reprocell #RCAB001P2P) for 1h at RT, followed by 3 washes with 3% BSA in PBST (PBS + 0.1% Triton) and a secondary Alexa Fluor 488 donkey anti-rabbit IgG (H+L) (Thermo Fisher #A21206) for another hour at RT. The cell suspension was then filtered through a BD Falcon 12 × 75–mm tube with a cell strainer cap (BD Falcon

#352235) and analyzed on a BD Fortessa flow cytometer. Data was plotted with FlowJo v.10 and the positive gate was set according to a secondary antibody only negative control.

S1 Nuclease Assay—Exponentially growing cells on reprogramming day 10 or established iPS cell lines were pulse-labeled with 30 μM IdU for 15 min, washed with PBS twice, and exposed to 150 μM CldU for 45 min. After exposure to the second nucleotide analog, cells were collected, washed in 1x PBS and permeabilized with CSK buffer (100mM NaCl, 10mM MOPS pH7, 3mM $MgCl_2$, 300mM sucrose and 0.05% Triton X-100 in water) for 10 min on ice and centrifuged at ~4,600g for 5 min at 4°C. Permeabilized cells were then treated with 100μl of S1 buffer (30mM sodium acetate pH4.6, 10mM zinc acetate, 5% glycerol, 50mM NaCl in water) with or without the S1 nuclease (Thermo Fisher Scientific #18001–016) at 10U/ml for 15 min at 37°C. Cells were pelleted at ~4,600g for 5 min at 4°C and then resuspended in PBS. Labeled cells were harvested and resuspended in PBS at a concentration of 2×10^5 cells/ml. Two microliters of cell suspension were spotted onto a pre-cleaned glass slide and lysed with 10μl of spreading buffer (0.5% SDS in 200mM Tris-HCl, pH7.4 and 50mM EDTA). After 6min, the slides were tilted at 15° relative to a horizontal surface, allowing the DNA fibers to spread. Slides were air-dried, fixed in methanol and acetic acid (3:1) for 2 min, rehydrated in PBS for 10 min and denatured with 2.5M HCl for 50 min at room temperature. Slides were then rinsed in PBS and blocked in PBS + 0.1% Triton X-100 (PBST) + 5% BSA for 1h at RT. Rat anti-BrdU (1:100, Abcam #ab6326) and mouse anti-BrdU (1:100, Becton Dickinson #347580) were then applied to detect CldU and IdU, respectively. After a 1h incubation, slides were washed in PBS and stained with Alexa Fluor 488-labeled goat anti-mouse IgG1 antibody and Alexa Fluor 594-labeled goat anti-rat antibody (1:300 each, Thermo Fisher Scientific). Slides were mounted in Prolong Gold Antifade (Thermo Fisher Scientific #P10144) and stored at −20°C. Replication tracks were imaged on a Nikon Eclipse 90i microscope, fitted with a PL Apo 40X/0.95 numerical aperture (NA) objective. The length of each track was determined manually using the segmented line tool on ImageJ software (NIH). The pixel values were converted into μm using the scale bar generated by the microscope software. Size distribution of track lengths from individual DNA fibers was plotted as scatter dot plot with a line representing the median.

QUANTIFICATION AND STATISTICAL ANALYSIS

Each genotype in an experiment was present in at least 3 biological replicates (MEFs from different embryos of the same genotype). Samples with only two biological replicates were not used for statistical analysis or to solely base conclusions on, and are instead shown as affirming results with other genotypes.

Statistical calculations were carried out with GraphPad Prism. Comparisons between multiple experimental groups or genotypes were performed with one-way ANOVA and analyzed with Sidak's multiple comparisons test. For all ANOVA analyses, CI = 95%. In the cases where only two experimental groups were available, statistical significance was evaluated with a two-tailed, unpaired student's t-test. Statistically significant differences in DNA fiber track length distributions in the S1 nuclease assay were determined by a Mann-Whitney test. *$p < 0.05$, **$p < 0.01$ and ***$p < 0.001$ and ****$p < 0.0001$. All error

bars represent the standard error of the mean (SEM). Figures were prepared with Adobe Illustrator, the Graphical Abstract was made with Biorender.

Supplementary Material

Refer to Web version on PubMed Central for supplementary material.

ACKNOWLEDGEMENTS

We thank Jean Gautier and Claudia Doege for comments and experimental suggestions, Thomas Ludwig for generating and providing the *Abraxas*^{S404A} and *Bach1*^{S994A} single mutant mouse strains, which are being used for independent studies on tumorigenesis, Foon Wu-Baer and David Billing for sharing mouse strains and MEF lines and Silvia Alvarez Nanez for training in DNA fiber analysis. This study was supported by 1R01GM132604-01A1 (DE) and R21 HG010165-01A1 (DE), NYSTEM IDEA award #C32564GG (DE), R01CA197774 (AC), R01CA227450 (AC and RB), and P01CA174653 (AC and RB), by the Diabetes Research Center Flow Core Facility Center Grant P30DK063608 and Flow Cytometry Core Facility grant gg015965-01 5r01gm132604-02. CRR was supported by fellowships from the National Cancer Institute (T32-CA09503) and the DoD Breast Cancer Research Program (BC083089). MH was supported by the JSPS Overseas Research Fellowship (JSPS-2016180) and the Uehara Memorial Foundation Research Fellowship (201740041).

REFERENCES

1. Takahashi K, and Yamanaka S (2006). Induction of pluripotent stem cells from mouse embryonic and adult fibroblast cultures by defined factors. Cell 126, 663–676. [PubMed: 16904174]
2. Gonzalez F, Georgieva D, Vanoli F, Shi ZD, Stadtfeld M, Ludwig T, Jasin M, and Huangfu D (2013). Homologous recombination DNA repair genes play a critical role in reprogramming to a pluripotent state. Cell Rep 3, 651–660. S2211–1247(13)00064–8 [pii] 10.1016/j.celrep.2013.02.005 [doi]. [PubMed: 23478019]
3. Ruiz S, Lopez-Contreras AJ, Gabut M, Marion RM, Gutierrez-Martinez P, Bua S, Ramirez O, Olalde I, Rodrigo-Perez S, Li H, et al. (2015). Limiting replication stress during somatic cell reprogramming reduces genomic instability in induced pluripotent stem cells. Nat Commun 6, 8036. 10.1038/ncomms9036. [PubMed: 26292731]
4. Muller LU, Milsom MD, Harris CE, Vyas R, Brumme KM, Parmar K, Moreau LA, Schambach A, Park IH, London WB, et al. (2012). Overcoming reprogramming resistance of Fanconi anemia cells. Blood 119, 5449–5457. blood-2012-02-408674 [pii] 10.1182/blood-2012-02-408674 [doi]. [PubMed: 22371882]
5. Chia G, Agudo J, Treff N, Sauer MV, Billing D, Brown BD, Baer R, and Egli D (2017). Genomic instability during reprogramming by nuclear transfer is DNA replication dependent. Nat Cell Biol 19, 282–291. 10.1038/ncb3485. [PubMed: 28263958]
6. Gomez-Cabello D, Checa-Rodriguez C, Abad M, Serrano M, and Huertas P (2017). CtIP-Specific Roles during Cell Reprogramming Have Long-Term Consequences in the Survival and Fitness of Induced Pluripotent Stem Cells. Stem Cell Reports 8, 432–445. 10.1016/j.stemcr.2016.12.009. [PubMed: 28065643]
7. Raya A, Rodriguez-Piza I,R, Guillermo G, Vassena R, and Navarro S (2009). Disease-corrected haematopoietic progenitors from Fanconi anaemia induced pluripotent stem cells. Nature 460, 53–59. [PubMed: 19483674]
8. Kinoshita T, Nagamatsu G, Kosaka T, Takubo K, Hotta A, Ellis J, and Suda T (2011). Ataxia-telangiectasia mutated (ATM) deficiency decreases reprogramming efficiency and leads to genomic instability in iPS cells. Biochem Biophys Res Commun 407, 321–326. 10.1016/j.bbrc.2011.03.013. [PubMed: 21385566]
9. Utikal J, Polo JM, Stadtfeld M, Maherali N, Kulalert W, Walsh RM, Khalil A, Rheinwald J, and Hochedlinger K (2009). Immortalization eliminates a roadblock during cellular reprogramming into iPS cells. Nature 460, Nature. 2009 Aug 2027;2460(7259):1145–2008. doi: 10.1038/nature08285. Epub 02009 Aug 08289.

10. Hong H, Takahashi K, Ichisaka T, Aoi T, Kanagawa O, Nakagawa M, Okita K, and Yamanaka S (2009). Suppression of Induced Pluripotent Stem Cell Generation by the p53-p21 Pathway. Nature 460, 1132–1134. [PubMed: 19668191]

11. Kawamura T, Suzuki J, Wang Y, Menendez S, Morera L, Raya A, Wahl G, and Izpisúa Belmonte J (2009). Linking the p53 tumour suppressor pathway to somatic cell reprogramming. Nature 460, 1140–1144. [PubMed: 19668186]

12. Kareta MS, Gorges LL, Hafeez S, Benayoun BA, Marro S, Zmoos AF, Cecchini MJ, Spacek D, Batista LF, O'Brien M, et al. (2015). Inhibition of pluripotency networks by the Rb tumor suppressor restricts reprogramming and tumorigenesis. Cell Stem Cell 16, 39–50. 10.1016/j.stem.2014.10.019. [PubMed: 25467916]

13. Moynahan ME, Chiu JW, Koller B, and Maria Jasin M (1999). Brca1 Controls Homology-Directed DNA Repair. Molecular Cell 4.

14. Chen CC, Feng W, Lim PX, Kass EM, and Jasin M (2018). Homology-Directed Repair and the Role of BRCA1, BRCA2, and Related Proteins in Genome Integrity and Cancer. Annu Rev Cancer Biol 2, 313–336. 10.1146/annurev-cancerbio-030617-050502. [PubMed: 30345412]

15. Bunting SF, Callen E, Wong N, Chen HT, Polato F, Gunn A, Bothmer A, Feldhahn N, Fernandez-Capetillo O, Cao L, et al. (2010). 53BP1 inhibits homologous recombination in Brca1-deficient cells by blocking resection of DNA breaks. Cell 141, 243–254. 10.1016/j.cell.2010.03.012. [PubMed: 20362325]

16. Setiaputra D, and Durocher D (2019). Shieldin - the protector of DNA ends. EMBO Rep 20. 10.15252/embr.201847560.

17. Schlacher K, Wu H, and Jasin M (2012). A distinct replication fork protection pathway connects Fanconi anemia tumor suppressors to RAD51-BRCA1/2. Cancer Cell 22, 106–116. 10.1016/j.ccr.2012.05.015. [PubMed: 22789542]

18. Pathania S, Bade S, Le Guillou M, Burke K, Reed R, Bowman-Colin C, Su Y, Ting DT, Polyak K, Richardson AL, et al. (2014). BRCA1 haploinsufficiency for replication stress suppression in primary cells. Nat Commun 5, 5496. 10.1038/ncomms6496. [PubMed: 25400221]

19. Billing D, Horiguchi M, Wu-Baer F, Taglialatela A, Leuzzi G, Nanez SA, Jiang W, Zha S, Szabolcs M, Lin CS, et al. (2018). The BRCT Domains of the BRCA1 and BARD1 Tumor Suppressors Differentially Regulate Homology-Directed Repair and Stalled Fork Protection. Mol Cell 72, 127–139 e128. 10.1016/j.molcel.2018.08.016. [PubMed: 30244837]

20. Mason JM, Chan YL, Weichselbaum RW, and Bishop DK (2019). Non-enzymatic roles of human RAD51 at stalled replication forks. Nat Commun 10, 4410. 10.1038/s41467-019-12297-0. [PubMed: 31562309]

21. Przetocka S, Porro A, Bolck HA, Walker C, Lezaja A, Trenner A, von Aesch C, Himmels SF, D'Andrea AD, Ceccaldi R, et al. (2018). CtIP-Mediated Fork Protection Synergizes with BRCA1 to Suppress Genomic Instability upon DNA Replication Stress. Mol Cell 72, 568–582 e566. 10.1016/j.molcel.2018.09.014. [PubMed: 30344097]

22. Schlacher K, Christ N, Siaud N, Egashira A, Wu H, and Jasin M (2011). Double-strand break repair-independent role for BRCA2 in blocking stalled replication fork degradation by MRE11. Cell 145, 529–542. 10.1016/j.cell.2011.03.041. [PubMed: 21565612]

23. Taglialatela A, Leuzzi G, Sannino V, Cuella-Martin R, Huang JW, Wu-Baer F, Baer R, Costanzo V, and Ciccia A (2021). REV1-Polzeta maintains the viability of homologous recombination-deficient cancer cells through mutagenic repair of PRIMPOL-dependent ssDNA gaps. Mol Cell 81, 4008–4025 e4007. 10.1016/j.molcel.2021.08.016. [PubMed: 34508659]

24. Panzarino NJ, Krais JJ, Cong K, Peng M, Mosqueda M, Nayak SU, Bond SM, Calvo JA, Doshi MB, Bere M, et al. (2020). Replication Gaps Underlie BRCA-deficiency and Therapy Response. Cancer Res. 10.1158/0008-5472.CAN-20-1602.

25. Kang Z, Fu P, Alcivar AL, Fu H, Redon C, Foo TK, Zuo Y, Ye C, Baxley R, Madireddy A, et al. (2021). BRCA2 associates with MCM10 to suppress PRIMPOL-mediated repriming and single-stranded gap formation after DNA damage. Nat Commun 12, 5966. 10.1038/s41467-021-26227-6. [PubMed: 34645815]

26. Quinet A, Tirman S, Jackson J, Šviković S, Lemaçon D, Carvajal-Maldonado D, González-Acosta D, Vessoni AT, Cybulla E, Wood M, et al. (2020). PRIMPOL-Mediated Adaptive Response

Suppresses Replication Fork Reversal in BRCA-Deficient Cells. Mol Cell 77, 461–474.e469. 10.1016/j.molcel.2019.10.008. [PubMed: 31676232]

27. Ludwig T, Fisher P, Ganesan S, and Efstratiadis A (2001). Tumorigenesis in mice carrying a truncating Brca1 mutation. Genes Dev 15, 1188–1193. 10.1101/gad.879201. [PubMed: 11358863]
28. Shakya R, Reid L, Reczek C, Cole F, Egli D, Lin C, deRooij D, Hirsch S, Ravi K, Hicks J, et al. (2011). BRCA1 Tumor Suppression Depends on BRCT Phosphoprotein Binding, But Not Its E3 Ligase Activity. Science 334, 525–527. [PubMed: 22034435]
29. Wang B, Matsuoka S, Ballif BA, Zhang D, Smogorzewska A, Gygi SP, and Elledge SJ (2007). Abraxas and RAP80 form a BRCA1 protein complex required for the DNA damage response. Science 316, 1194–1198. 10.1126/science.1139476. [PubMed: 17525340]
30. Cantor S, Bell D, Ganesan S, Kass E, Drapkin R, Grossman S, Wahrer D, Sgroi D, Lane W, Haber D, and Livingston D (2001). BACH1, a Novel Helicase-like Protein, Interacts Directly with BRCA1 and Contributes to Its DNA Repair Function. Cell 105, 149–160. [PubMed: 11301010]
31. Yu XW,L; Bowcock A; Aronheim A; Baer R (1998). The C-terminal (BRCT) Domains of BRCA1 Interact in Vivo with CtIP, a Protein Implicated in the CtBP Pathway of Transcriptional Repression. The Journal of Biological Chemistry Vol. 273, 25388–25392. [PubMed: 9738006]
32. Mateos-Gomez PA, Kent T, Deng SK, McDevitt S, Kashkina E, Hoang TM, Pomerantz RT, and Sfeir A (2017). The helicase domain of Poltheta counteracts RPA to promote alt-NHEJ. Nat Struct Mol Biol 24, 1116–1123. 10.1038/nsmb.3494. [PubMed: 29058711]
33. Wu L, Wang Z, Tsan J, Spillman M, Phung A, Xu X, Yang M, Hwang L, Bowcock A, and Baer R (1996). Identification of a RING protein that can interact *in vivo* with the *BRCA1* gene product. Nature Genetics 14, 430–440. [PubMed: 8944023]
34. Li M, and Yu X (2013). Function of BRCA1 in the DNA damage response is mediated by ADP-ribosylation. Cancer Cell 23, 693–704. 10.1016/j.ccr.2013.03.025. [PubMed: 23680151]
35. Vassin VM, Anantha RW, Sokolova E, Kanner S, and Borowiec JA (2009). Human RPA phosphorylation by ATR stimulates DNA synthesis and prevents ssDNA accumulation during DNA-replication stress. J Cell Sci 122, 4070–4080. 10.1242/jcs.053702. [PubMed: 19843584]
36. Murphy AK, Fitzgerald M, Ro T, Kim JH, Rabinowitsch AI, Chowdhury D, Schildkraut CL, and Borowiec JA (2014). Phosphorylated RPA recruits PALB2 to stalled DNA replication forks to facilitate fork recovery. J Cell Biol 206, 493–507. 10.1083/jcb.201404111. [PubMed: 25113031]
37. Joseph SA, Taglialatela A, Leuzzi G, Huang JW, Cuella-Martin R, and Ciccia A (2020). Time for remodeling: SNF2-family DNA translocases in replication fork metabolism and human disease. DNA Repair (Amst) 95, 102943. 10.1016/j.dnarep.2020.102943. [PubMed: 32971328]
38. Taglialatela A, Alvarez S, Leuzzi G, Sannino V, Ranjha L, Huang JW, Madubata C, Anand R, Levy B, Rabadan R, et al. (2017). Restoration of Replication Fork Stability in BRCA1- and BRCA2-Deficient Cells by Inactivation of SNF2-Family Fork Remodelers. Mol Cell 68, 414–430 e418. 10.1016/j.molcel.2017.09.036. [PubMed: 29053959]
39. Rodriguez R, Muller S, Yeoman JA, Trentesaux C, Riou JF, and Balasubramanian S (2008). A novel small molecule that alters shelterin integrity and triggers a DNA-damage response at telomeres. J Am Chem Soc 130, 15758–15759. 10.1021/ja805615w. [PubMed: 18975896]
40. Mirman Z d.L. T (2020). 53BP1: a DSB escort. Genes & Development 34, 7–23. 10.1101/gad.333237. [PubMed: 31896689]
41. Bouwman P, Aly A, Escandell JM, Pieterse M, Bartkova J, van der Gulden H, Hiddingh S, Thanasoula M, Kulkarni A, Yang Q, et al. (2010). 53BP1 loss rescues BRCA1 deficiency and is associated with triple-negative and BRCA-mutated breast cancers. Nat Struct Mol Biol 17, 688–695. 10.1038/nsmb.1831. [PubMed: 20453858]
42. Liu WK,A; Zhao R; Cortez D (2020). Two replication fork remodeling pathways generate nuclease substrates for distinct fork protection factors. Science Advances
43. Cuella-Martin R, Oliveira C, Lockstone HE, Snellenberg S, Grolmusova N, and Chapman JR (2016). 53BP1 Integrates DNA Repair and p53-Dependent Cell Fate Decisions via Distinct Mechanisms. Mol Cell 64, 51–64. 10.1016/j.molcel.2016.08.002. [PubMed: 27546791]
44. Ward IM, Difilippantonio S, Minn K, Mueller MD, Molina JR, Yu X, Frisk CS, Ried T, Nussenzweig A, and Chen J (2005). 53BP1 cooperates with p53 and functions as

a haploinsufficient tumor suppressor in mice. Mol Cell Biol 25, 10079–10086. 10.1128/MCB.25.22.10079-10086.2005. [PubMed: 16260621]

45. Balestrini A, Ristic D, Dionne I, Liu XZ, Wyman C, Wellinger RJ, and Petrini JH (2013). The Ku heterodimer and the metabolism of single-ended DNA double-strand breaks. Cell Rep 3, 2033–2045. 10.1016/j.celrep.2013.05.026. [PubMed: 23770241]
46. Shao RG, Cao CX, Zhang H, Kohn KW, Wold MS, and Pommier Y (1999). Replication-mediated DNA damage by camptothecin induces phosphorylation of RPA by DNA-dependent protein kinase and dissociates RPA:DNA-PK complexes. Embo j 18, 1397–1406. 10.1093/emboj/18.5.1397. [PubMed: 10064605]
47. Strumberg D, Pilon AA, Smith M, Hickey R, Malkas L, and Pommier Y (2000). Conversion of topoisomerase I cleavage complexes on the leading strand of ribosomal DNA into 5'-phosphorylated DNA double-strand breaks by replication runoff. Mol Cell Biol 20, 3977–3987. 10.1128/mcb.20.11.3977-3987.2000. [PubMed: 10805740]
48. Rothkamm K, Kruger I, Thompson LH, and Lobrich M (2003). Pathways of DNA double-strand break repair during the mammalian cell cycle. Mol Cell Biol 23, 5706–5715. [PubMed: 12897142]
49. Glover TB,C; Coyle J; Echo B (1984). DNA polymerase a inhibition by aphidicolin induces gaps and breaks at common fragile sites in human chromosomes. Hum Genetics 67, 136–142.
50. Strumberg D, Pilon A, Smith M, Hickey R, Malkas L, and Pommier Y (2000). Conversion of Topoisomerase I Cleavage Complexes on the Leading Strand of Ribosomal DNA into 5'-Phosphorylated DNA Double-Strand Breaks by Replication Runoff. MOLECULAR AND CELLULAR BIOLOGY 20, 3977–3987. [PubMed: 10805740]
51. Doege CA, Inoue K, Yamashita T, Rhee DB, Travis S, Fujita R, Guarnieri P, Bhagat G, Vanti WB, Shih A, et al. (2012). Early-stage epigenetic modification during somatic cell reprogramming by Parp1 and Tet2. Nature 488, 652–655. nature11333 [pii] 10.1038/nature11333 [doi]. [PubMed: 22902501]
52. Farmer H, McCabe N, Lord C, Tutt A, Johnson D, Richardson T, Santarosa M, Dillon K, Hickson I, Knights C, et al. (2005). Targeting the DNA repair defect in BRCA mutant cells as a therapeutic strategy. Nature 434, 917–921. [PubMed: 15829967]
53. Bryant H, Schultz N, Thomas H, Parker K, Flower D, Lopez E, Kyle S, Meuth M, Curtin N, and Helleday T (2005). Specific killing of BRCA2-deficient tumours with inhibitors of poly(ADP-ribose) polymerase. Nature 434, 913–917. [PubMed: 15829966]
54. Hanzlikova H, Kalasova I, Demin AA, Pennicott LE, Cihlarova Z, and Caldecott KW (2018). The Importance of Poly(ADP-Ribose) Polymerase as a Sensor of Unligated Okazaki Fragments during DNA Replication. Mol Cell 71, 319–331 e313. 10.1016/j.molcel.2018.06.004. [PubMed: 29983321]
55. Cong K, Peng M, Kousholt AN, Lee WTC, Lee S, Nayak S, Krais J, VanderVere-Carozza PS, Pawelczak KS, Calvo J, et al. (2021). Replication gaps are a key determinant of PARP inhibitor synthetic lethality with BRCA deficiency. Mol Cell 81, 3128–3144 e3127. 10.1016/j.molcel.2021.06.011. [PubMed: 34216544]
56. Ward IM, Minn K, van Deursen J, and Chen J (2003). p53 Binding protein 53BP1 is required for DNA damage responses and tumor suppression in mice. Mol Cell Biol 23, 2556–2563. [PubMed: 12640136]
57. Quinet A, Martins DJ, Vessoni AT, Biard D, Sarasin A, Stary A, and Menck CF (2016). Translesion synthesis mechanisms depend on the nature of DNA damage in UV-irradiated human cells. Nucleic Acids Res 44, 5717–5731. 10.1093/nar/gkw280. [PubMed: 27095204]
58. Lim PX, Zaman M, Feng W, and Jasin M (2024). BRCA2 promotes genomic integrity and therapy resistance primarily through its role in homology-directed repair. Mol Cell 84, 447–462.e410. 10.1016/j.molcel.2023.12.025. [PubMed: 38244544]
59. Lim PX, Zaman M, and Jasin M (2023). BRCA2 promotes genomic integrity and therapy resistance primarily through its role in homology-directed repair. bioRxiv. 10.1101/2023.04.11.536470.
60. Brumbaugh J, Di Stefano B, and Hochedlinger K (2019). Reprogramming: identifying the mechanisms that safeguard cell identity. Development 146. 10.1242/dev.182170.

61. Ryan AJ, Squires S, Strutt HL, and Johnson RT (1991). Camptothecin cytotoxicity in mammalian cells is associated with the induction of persistent double strand breaks in replicating DNA. Nucleic Acids Res 19, 3295–3300. 10.1093/nar/19.12.3295. [PubMed: 1905803]
62. Ben-Porath I, Thomson MW, Carey VJ, Ge R, Bell GW, Regev A, and Weinberg RA (2008). An embryonic stem cell-like gene expression signature in poorly differentiated aggressive human tumors. Nat Genet 40, 499–507. 10.1038/ng.127. [PubMed: 18443585]
63. Bartkova J, Rezaei N, Liontos M, Karakaidos P, Kletsas D, Issaeva N, Vassiliou LV, Kolettas E, Niforou K, Zoumpourlis VC, et al. (2006). Oncogene-induced senescence is part of the tumorigenesis barrier imposed by DNA damage checkpoints. Nature 444, 633–637. nature05268 [pii] 10.1038/nature05268 [doi]. [PubMed: 17136093]
64. Moreno A, Carrington JT, Albergante L, Al Mamun M, Haagensen EJ, Komseli ES, Gorgoulis VG, Newman TJ, and Blow JJ (2016). Unreplicated DNA remaining from unperturbed S phases passes through mitosis for resolution in daughter cells. Proc Natl Acad Sci U S A 113, E5757–5764. 10.1073/pnas.1603252113. [PubMed: 27516545]
65. Lezaja A, and Altmeyer M (2018). Inherited DNA lesions determine G1 duration in the next cell cycle. Cell Cycle 17, 24–32. 10.1080/15384101.2017.1383578. [PubMed: 28980862]
66. Moser J, Miller I, Carter D, and Spencer SL (2018). Control of the Restriction Point by Rb and p21. Proc Natl Acad Sci U S A 115, E8219–e8227. 10.1073/pnas.1722446115. [PubMed: 30111539]
67. Hussein SM, Batada NN, Vuoristo S, Ching RW, Autio R, Narva E, Ng S, Sourour M, Hamalainen R, Olsson C, et al. (2011). Copy number variation and selection during reprogramming to pluripotency. Nature 471, 58–62. nature09871 [pii] 10.1038/nature09871 [doi]. [PubMed: 21368824]
68. Mandai M, Watanabe A, Kurimoto Y, Hirami Y, Morinaga C, Daimon T, Fujihara M, Akimaru H, Sakai N, Shibata Y, et al. (2017). Autologous Induced Stem-Cell–Derived Retinal Cells for Macular Degeneration. New England Journal of Medicine 376, 1038–1046. 10.1056/NEJMoa1608368. [PubMed: 28296613]
69. Reczek CR, Szabolcs M, Stark JM, Ludwig T, and Baer R (2013). The interaction between CtIP and BRCA1 is not essential for resection-mediated DNA repair or tumor suppression. J Cell Biol 201, 693–707. 10.1083/jcb.201302145. [PubMed: 23712259]
70. Durkin MQ,X; Popescu N; Lowy D (2013). Isolation of Mouse Embryo Fibroblasts. Bio Protoc 3.
71. Anantha RW, Vassin VM, and Borowiec JA (2007). Sequential and synergistic modification of human RPA stimulates chromosomal DNA repair. J Biol Chem 282, 35910–35923. 10.1074/jbc.M704645200. [PubMed: 17928296]
72. Orlando L, Tanasijevic B, Nakanishi M, Reid JC, García-Rodríguez JL, Chauhan KD, Porras DP, Aslostovar L, Lu JD, Shapovalova Z, et al. (2021). Phosphorylation state of the histone variant H2A.X controls human stem and progenitor cell fate decisions. Cell Rep 34, 108818. 10.1016/j.celrep.2021.108818. [PubMed: 33691101]
73. Palmerola KL, Amrane S, De Los Angeles A, Xu S, Wang N, de Pinho J, Zuccaro MV, Taglialatela A, Massey DJ, Turocy J, et al. (2022). Replication stress impairs chromosome segregation and preimplantation development in human embryos. Cell 185, 2988–3007.e2920. 10.1016/j.cell.2022.06.028. [PubMed: 35858625]
74. Terret ME, Sherwood R, Rahman S, Qin J, and Jallepalli PV (2009). Cohesin acetylation speeds the replication fork. Nature 462, 231–234. nature08550 [pii] 10.1038/nature08550 [doi]. [PubMed: 19907496]

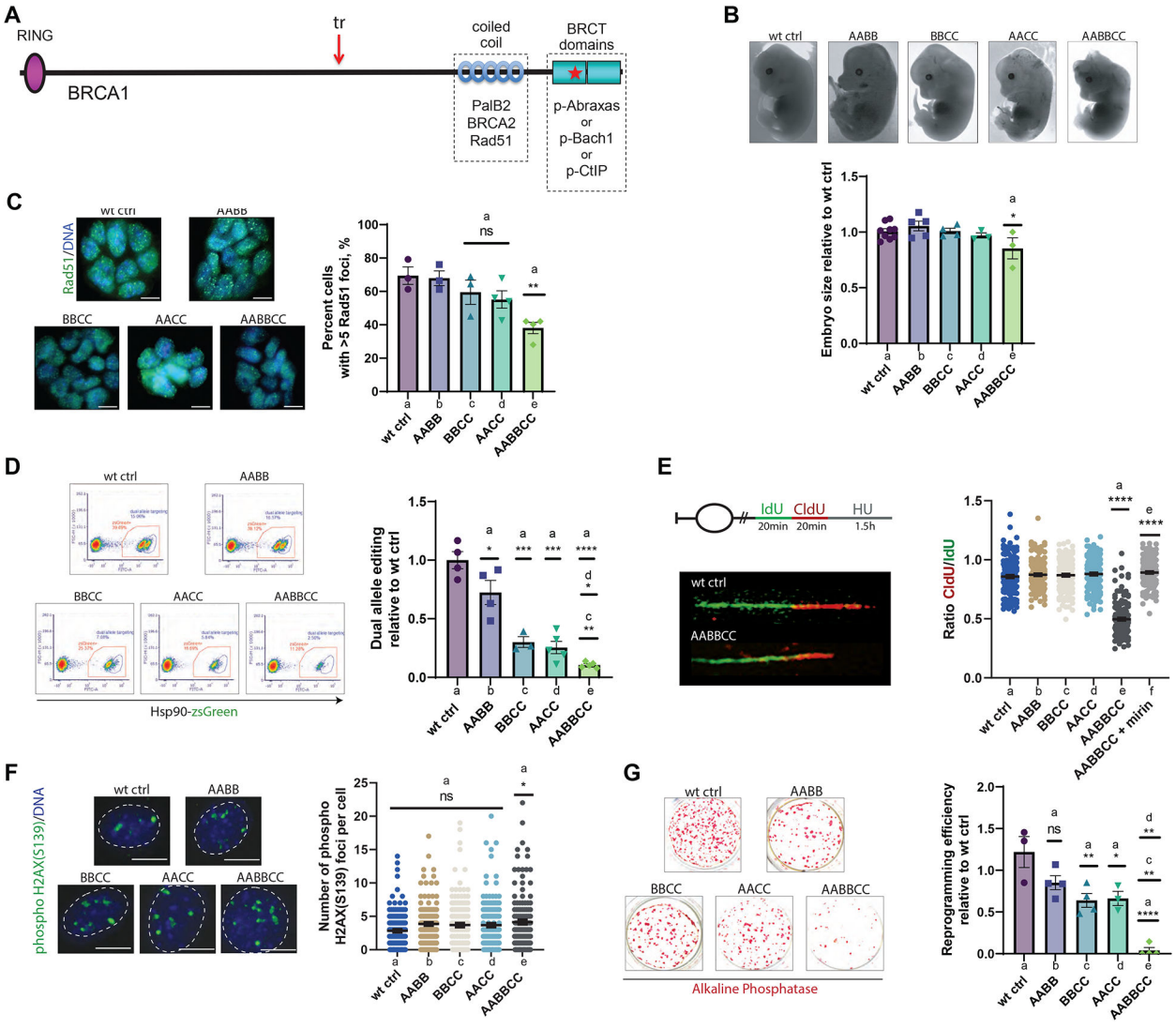

Figure 1. Phosphoprotein interaction of Brca1 with Abraxas, Bach1 and CtIP is required for HDR and reprogramming.

A) Illustration of the BRCA1 polypeptide and a simplified interaction engagements. The C-terminal BRCT domain of BRCA1 interacts in a mutually exclusive manner with the phosphorylated isoforms of ABRAXAS, BACH1, or CtIP to form distinct BRCA1 complexes. In addition, BRCA1 harbors a coiled-coil motif that mediates its interaction with PALB2 and the recruitment of BRCA2 and RAD51 to sites of DNA damage. The mutant mouse alleles used in this study: Brca1tr encodes a pathogenic truncating mutation, denoted with a red arrow, that eliminates the BRCT domains. AbraxasS404A, Bach1S994A and CtipS326A each encode a missense mutation that eliminates a phosphorylation site necessary for the interaction of its protein product with the BRCT domain of BRCA1. **B**) Morphology and size of E13.5 embryos. The difference between wt ctrl and AABBCC was evaluated with an unpaired two-tailed student's t-test.; wt ctrl n = 9, AABB n = 5, BBCC n = 4, AACC n = 3, AABBCC n = 3. **C**) Rad51 foci immunofluorescence and quantification in induced pluripotent stem (iPS) cell lines treated with 10Gy IR. Data was

analyzed by one-way ANOVA.; wt ctrl n = 3, AABB n =3, BBCC n = 3, AACC n = 4, AABBCC n = 4; A = Abraxas S404A/S404A, B = Bach1 S994A/S994A, C = CtIP S326A/S326A; scale bar = 10μm. **D**) CRISPR/Cas9 based HDR assay with induced pluripotent stem (iPS) cell lines, shown as a ratio of dual allele targeting in each genotype vs. control. Statistical analysis with one-way ANOVA, except for BBCC vs. AABBCC and AACC vs AABBCC, which used unpaired two-tailed student's t-tests.; wt ctrl n = 4, AABB n = 4, BBCC n = 3, AACC n = 5, AABBCC n= 5. **E**) DNA fork stalling in immortalized MEFs. At least 150 DNA fibers were measured per genotype. Analysis with one-way ANOVA. **F**) Immunofluorescence and quantification for phospho-H2AX (S139). Foci were counted on reprogramming day 5 in > 138 cells/genotype. Statistical analysis with one-way ANOVA. Size bar = 5μm, applicable to all panels. **G**) Alkaline phosphatase (AP) staining and reprogramming efficiency quantification. The number of AP positive colonies is shown as a ratio to wild type. Analysis by one-way ANOVA from biological replicates. wt ctrl n = 3, AABB n = 4, BBCC n = 4, AACC n = 3, AABBCC n = 4.

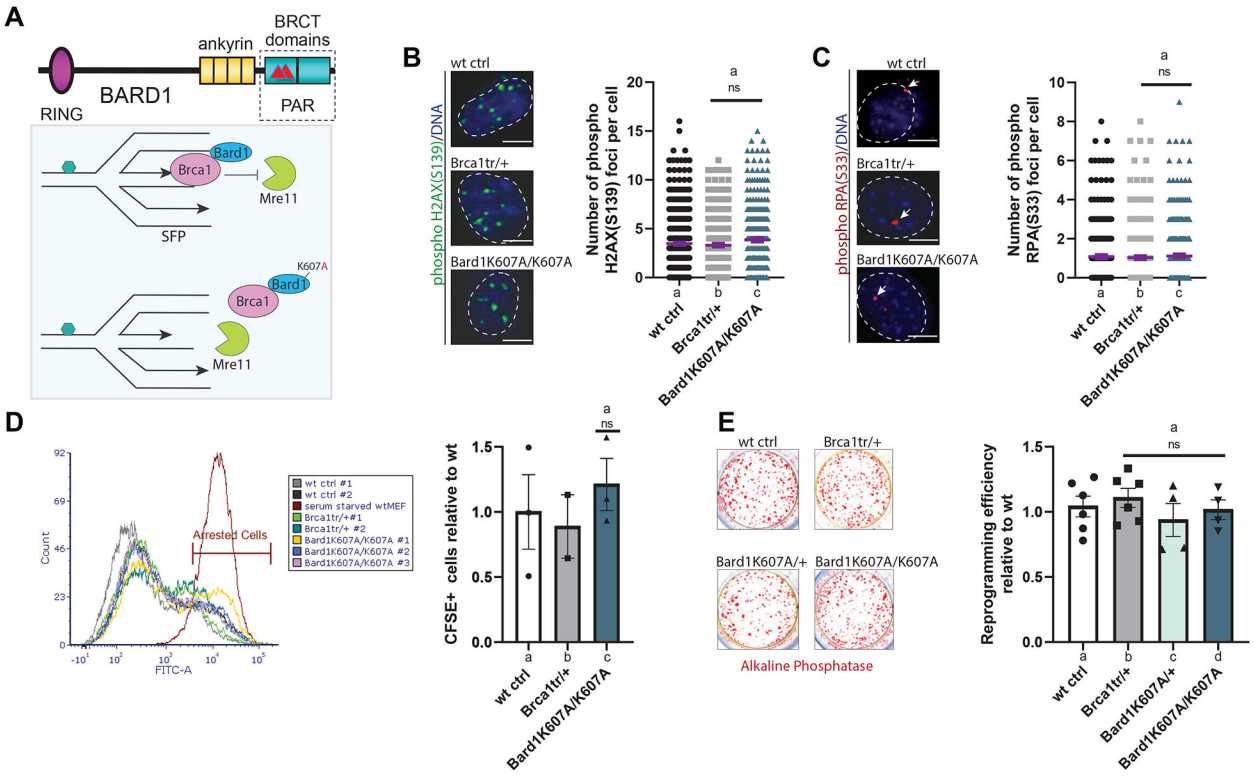

Figure 2. Stalled fork protection (SFP) is dispensable for reprogramming.
Related to Fig. S1.

A) A schematic of Bard1-mediated SFP. The Bard1^{K607A} point mutation prevents the recruitment of the Brca1/Bard1 heterodimer to reversed stalled replication forks, which makes them vulnerable to Mre11-dependent degradation. **B**) Immunofluorescence and quantification for double strand break (DSB) marker phospho - H2AX (S139). Foci were counted on reprogramming day 5 in ≥260 cells/genotype, statistical analysis with one-way ANOVA. scale bar = 5μm. **C**) Immunofluorescence and quantification of phospho -RPA(S33) on reprogramming day 5. Data from ≥240 cells/genotype and analyzed by one-way ANOVA.; The white arrows point to foci. scale bar = 5μm. **D**) Cell proliferation plots on reprogramming day 5. Arrested cells retain CFSE and are detectable as a bright peak by flow cytometry. Analysis by one-way ANOVA; wt ctrl n = 3, Brca1$^{tr/+}$ n = 2, Bard1$^{K607A/K607A}$ n = 3. **E**) Alkaline phosphatase (AP) staining and reprogramming efficiency quantification. The number of AP positive colonies is shown as a ratio to wild type. Analysis with one-way ANOVA.; wt ctrl n = 6, Brca1$^{tr/+}$ n = 6, Bard1$^{K607A/+}$ n = 4, Bard1$^{K607A/K607A}$ n = 4, n=biological replicates.

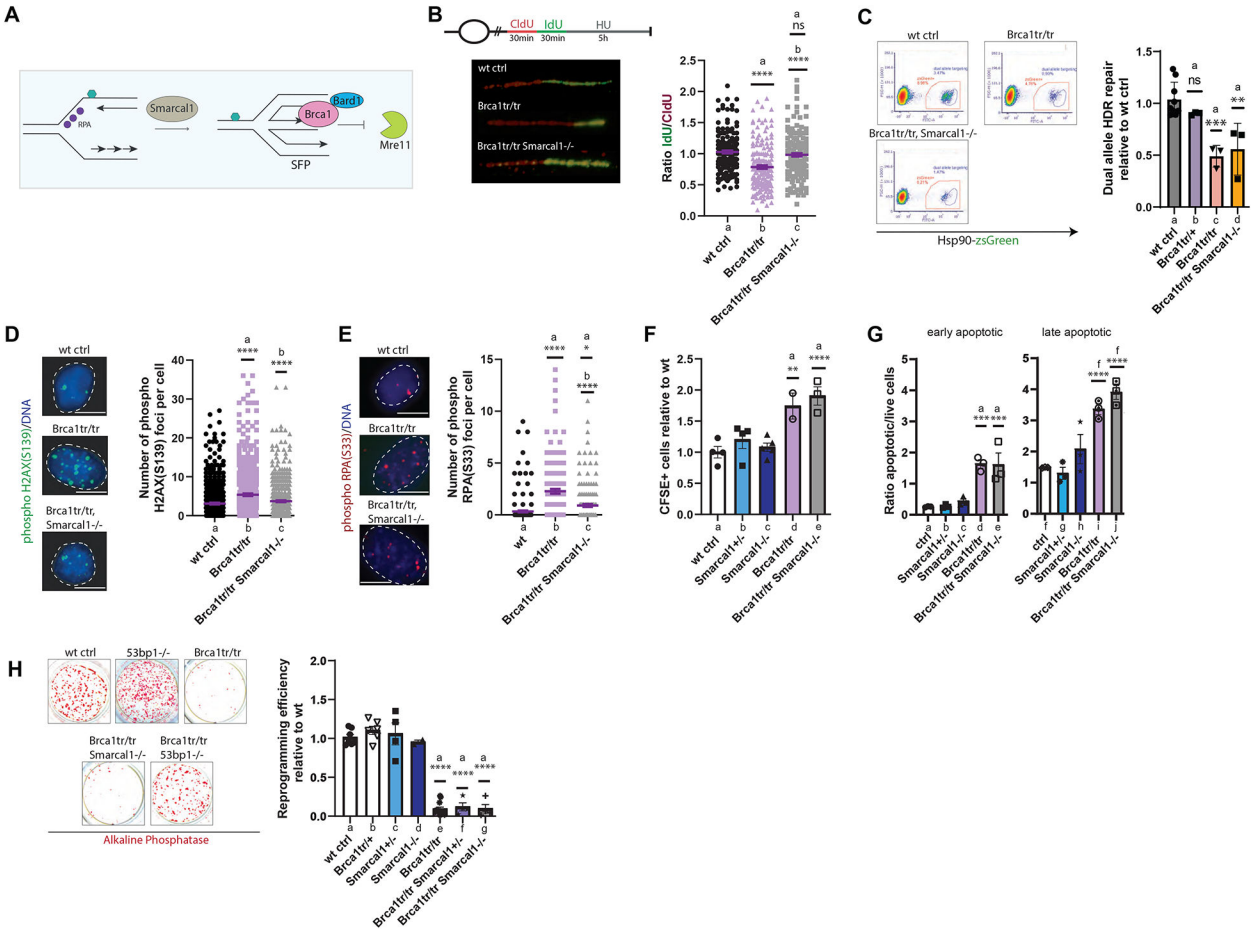

Figure 3. SFP-specific rescue of Brca1 function fails to restore reprogramming.

Related to Fig. S2

A) A schematic for rescuing SFP in BRCA1 mutant cells by ablation of Smarcal1. **B**) DNA fiber analysis in a fork stalling assay with hydroxyurea (HU) on reprogramming day 5. At least 120 DNA fibers were measured per genotype. Analysis by one-way ANOVA. **C**) CRISPR/Cas9 based HDR assay with induced pluripotent stem (iPS) cells lines. Data is shown as a ratio of dual allele targeting in each genotype relative to control. Statistical analysis with one-way ANOVA; wt ctrl n = 9, Brca1$^{tr/+}$ n = 3, Brca1$^{tr/tr}$ n = 3, Brca1$^{tr/tr}$ Smarcal1$^{-/-}$ n = 3. D) Immunofluorescence and quantification for double strand break (DSB) marker phospho-H2AX (S139). Foci were counted on reprogramming day 5 (≥410 cells/genotype) and statistical analysis performed with one-way ANOVA. **E**) Immunofluorescence and quantification of ssDNA marker phospho-RPA(S33) on reprogramming day 5. Data collected from ≥140 cells per genotype and analyzed by one-way ANOVA. **F**) Cell proliferation analysis with CFSE on reprogramming day 5. Statistical analysis with one-way ANOVA.; wt ctrl n = 4, Smarcal1$^{+/-}$ n = 4, Smarcal1$^{-/-}$ n = 5, Brca1$^{tr/tr}$ n = 2, Brca1$^{tr/tr}$ Smarcal1$^{-/-}$ n = 3. **G**) Apoptosis analysis with Annexin V and propidium iodide (PI) on reprogramming day 5. Analysis by one-way ANOVA.; wt ctrl n = 3, Smarcal1$^{+/-}$ n = 3, Smarcal1$^{-/-}$ n = 3, Brca1$^{tr/tr}$ n = 3, Brca1$^{tr/tr}$ Smarcal1$^{-/-}$ n = 3. **H**) Alkaline phosphatase (AP) staining and reprogramming efficiency quantification. The

number of AP positive colonies is shown as a ratio to wild type. Data analysis with one-way ANOVA.; wt ctrl n = 7, $Brca1^{tr/+}$ n = 6, $Smarcal1^{+/-}$ n = 4, $Smarcal1^{-/-}$ n = 2, $Brca1^{tr/tr}$ n = 12, $Brca1^{tr/tr}$ $Smarcal1^{+/-}$ n = 4, $Brca1^{tr/tr}$ $Smarcal1^{-/-}$ n = 4. n= biological replicates.

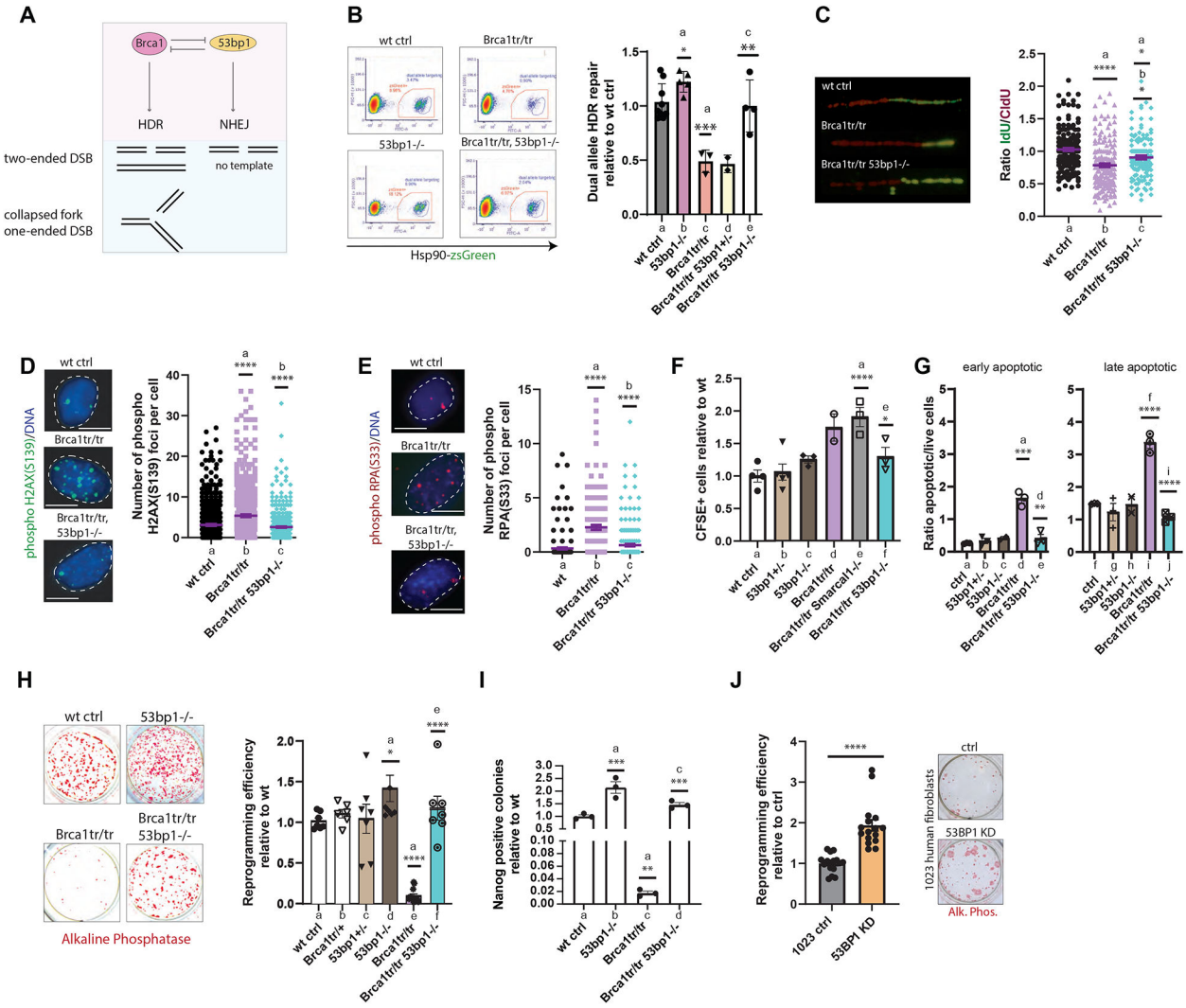

Figure 4. HDR-specific rescue of BRCA1 function restores reprogramming.
Related to Fig. S3.

A) A schematic for rescuing HDR in Brca1 mutant cells by ablation of 53bp1. Relevant substrates that can be repaired by HDR or NHEJ are shown. **B**) CRISPR/Cas9 based HDR assay with induced pluripotent stem (iPS) cells lines. Data is shown as a ratio of dual allele targeting in each genotype to dual allele targeting in the control. Statistical analysis using one-way ANOVA, except for the comparison between wt ctrl and 53bp1$^{-/-}$, evaluated with a two-tailed, unpaired student's t-test.; wt ctrl n = 9, Brca1$^{tr/+}$ n = 3, 53bp1$^{-/-}$ n = 5, Brca1$^{tr/tr}$ n = 3, Brca1$^{tr/tr}$53bp1$^{+/-}$ n = 2, Brca1$^{tr/tr}$53bp1$^{-/-}$ n = 4. **C**) DNA fiber analysis in a fork stalling assay with hydroxyurea (HU) on reprogramming day 5. At least 120 DNA fibers were measured per genotype and data was analyzed by one-way ANOVA. **D**) Immunofluorescence and quantification for phospho-H2AX (S139). Foci counted on reprogramming day 5 (≥410 cells/genotype), statistical analysis performed with one-way ANOVA. **E**) Immunofluorescence and quantification of ssDNA marker phospho RPA(S33) on reprogramming day 5. ≥140 cells per genotype, analyzed by one-way ANOVA. For control and BRCA1, images are identical for Fig. 3 and Fig. 4 for panels c and d. **F**) Cell

proliferation analysis with CFSE dye on reprogramming day 5. Statistics with one-way ANOVA.; wt ctrl n = 4,, 53bp1'/- n = 5, $53bp1^{-/-}$ n = 3, $Brca1^{tr/tr}$ n = 2, $Brca1^{tr/tr}Smarcal1^{-/-}$ n = 3, $Brca1^{tr/tr}$ $53bp1^{-/-}$ n = 3. **G**) Apoptosis analysis with Annexin V and propidium iodide (PI) on reprogramming day 5, analyzed by one-way ANOVA.; wt ctrl n = 3, $53bp1^{+/-}$ n = 3, $53bp1^{-/-}$ n = 2, $Brca1^{tr/tr}$ n = 3, $Brca1^{tr/tr}$ $53bp1^{-/-}$ n = 3. **H**) Alkaline phosphatase (AP) staining and reprogramming efficiency quantification. Number of AP positive colonies is shown as a ratio to wild type, analyzed with one-way ANOVA.; wt ctrl n = 7, $Brca1^{tr/+}$ n = 6, $53bp1^{+/-}$ n = 7, $53bp1^{-/-}$ n = 8, $Brca1^{tr/tr}$ n = 12, $Brca1^{tr/tr}$ $53bp1^{-/-}$ n = 7. **I**) Quantification of Nanog positive colonies in the indicated genotypes, analyzed with one-way ANOVA.; n = 3 for each genotype. **J**) AP staining and reprogramming efficiency quantification in human 1023 fibroblasts from adult skin biopsy in control and 53BP1 knockdown (KD) conditions. Cells were fixed on day 25 post reprogramming factor transduction, statistical analysis using an unpaired, two-tailed student's t-test.; ctrl n = 16, 53BP1 KD n = 16. Samples with n=2 are not used for statistical comparisons. All numbers indicated are biological replicates.

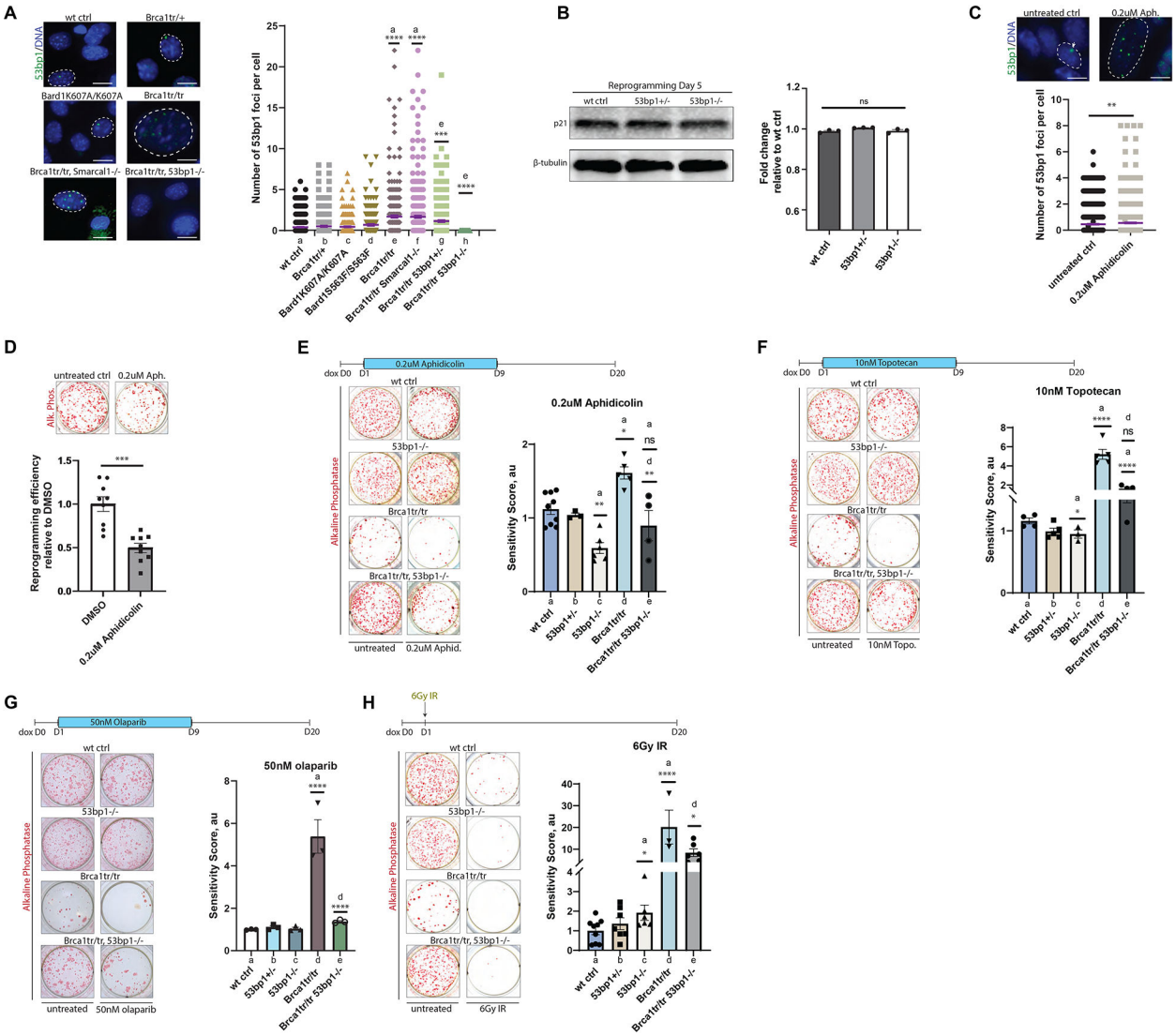

Figure 5. Replication-induced DNA double strand breaks limit reprogramming.

Related to Fig. S4.

A) Immunofluorescence of 53bp1 foci on reprogramming day 5. Data from at least 280 cells/genotype and analyzed by one-way ANOVA.; scale bar, 10μM. **B**) Western blot and signal quantification for p21 from cells of the indicated genotypes on reprogramming Day5. Analysis by one-way ANOVA; n = 3 for each genotype. **C**) Staining and quantification of 53bp1 foci in wild-type uninfected primary MEFs, treated with 0.2μM aphidicolin for 3 days. At least 1000 cells were analyzed per condition, statistical analysis using an unpaired two-tailed student's t-test.; scale bar, 10μM. **D**) Alkaline phosphatase (AP) staining of control and 0.2μM aphidicolin treated wild-type cells for 8 days during reprogramming. Analysis was performed with an unpaired, two-tailed student's t-test. n = 9 untreated, n = 9 aph. treated. **E-G**) A higher column is a greater sensitivity of the genotype to the drug applied. **E**) Alkaline phosphatase (AP) staining and genotype-specific sensitivity evaluation to treatment with 0.2μM aphidicolin for 8 days during reprogramming. Analysis by one-way ANOVA.; wt ctrl n = 9, $53bp1^{+/-}$ n = 3, $53bp1^{-/-}$ n = 6, $Brca1^{tr/tr}$ n = 5, $Brca1^{tr/tr}$ $53bp1^{-/-}$

n = 4. **F**) AP staining and genotype-specific sensitivity to treatment with 10nM topotecan for 8 days during reprogramming. Analysis by one-way ANOVA. The comparison between wt ctrl and 53bp1$^{-/-}$ was carried out with an unpaired two-tailed student's t-test.; wt ctrl n = 4, 53bp1$^{+/-}$ n = 5, 53bp1$^{-/-}$ n = 3, Brca1$^{tr/tr}$ n = 5, Brca1$^{tr/tr}$ 53bp1$^{-/-}$ n = 4. **G**) AP staining and genotype-specific sensitivity to treatment with 50nM olaparib for 8 days during reprogramming. Analysis by one-way ANOVA.; n = 3 for each genotype. **H**) AP staining and genotype-specific sensitivity to treatment with a single dose of 6Gy IR one day post reprogramming factor induction. Analysis by one-way ANOVA. The comparisons between wt ctrl and 53bp1$^{-/-}$ was carried out with an unpaired two-tailed student's t-test on biological replicates.; wt ctrl n = 9, 53bp1$^{+/-}$ n = 7, 53bp1$^{-/-}$ n = 6, Brca1$^{tr/tr}$ n = 3, Brca1$^{tr/tr}$ 53bp1$^{-/-}$ n = 6.

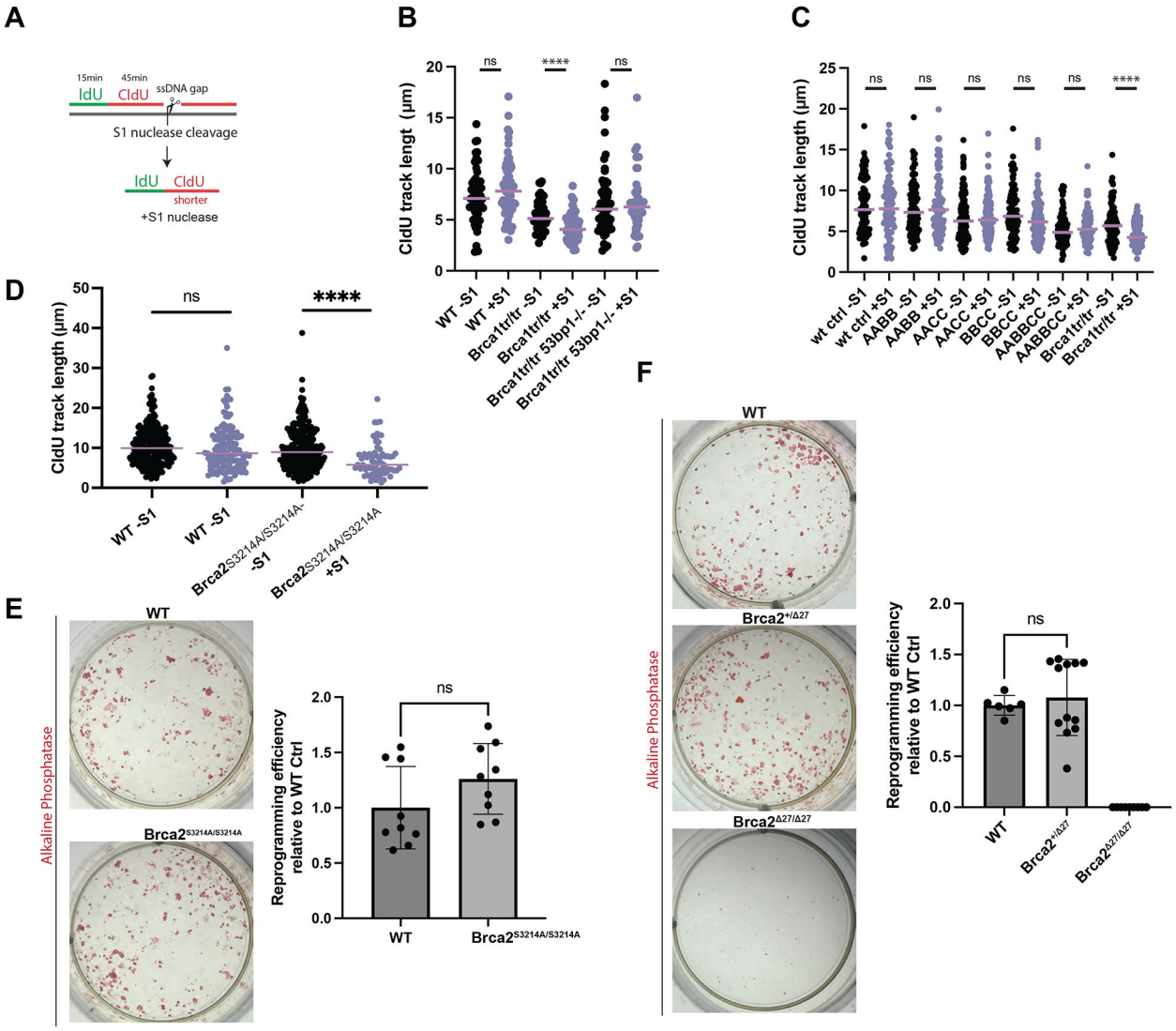

Figure 6. Replication gap suppression is not required for reprogramming.

Related to Fig. S4.

A) Schematic of replication gap evaluation with S1 nuclease. **B**) Dot plot of CldU track length in iPSC lines of the indicated genotypes; ≥ 100 fibers were measured per experimental condition. Analysis using a two-tailed Mann-Whitney test. Median track length marked by a purple line. **C**) Dot plot of CldU track length in iPSC lines of the indicated genotypes, collected from ≥ 50 fibers per condition and analyzed by a two-tailed Mann-Whitney test. **D**) Dot plot of CldU track length on reprogramming day 5 of the indicated genotypes; ≥ 100 fibers were measured per experimental condition. Analysis using a two-tailed Mann-Whitney test. **E**) AP staining of WT control and Brca2$^{S3214A/S3214A}$ cells of reprogramming. Analysis using an unpaired, two-tailed student's t-test. n = 10 for each genotype. **F**) AP staining and reprogramming efficiency quantification. The number of AP positive colonies is shown as a ratio to wild type. WT n=6, Brca2$^{+/\Delta 27}$ n=12, Brca2$^{\Delta 27/\Delta 27}$ n=9. Analysis using one-way ANOVA.

KEY RESOURCES TABLE

REAGENT or RESOURCE	SOURCE	IDENTIFIER
ANTIBODIES		
Sox2	Stemgent	Cat# 09–0024
rabbit-p21	Abcam	Cat# ab188224
rabbit α-alpha tubulin	Abcam	Cat# ab4074
Anti-phospho-Histone H2A.X-Ser139 mouse monoclonal Ab. Does not react to S139A in human pluripotent stem cells (Orlando et al., 2021).	Millipore	Cat# 05–636
rabbit αphospho-RPA2Ser33	Invitrogen	Cat# PA5–39809
α53BP1 H-300	Santa Cruz	Cat# 22760
rabbit αNanog	Reprocell	Cat#RCAB001P2P
Alexa Fluor 488 conjugated mouse αhuman TRA-1–60	BD Biosciences	Cat# BD560173
Purified mouse anti human 53BP1, clone 19	BD Transduction laboratories	Cat# 612522
Anti-Rad51 (Ab-1) Rabbit pAb.	EMD Millipore	Cat# PC130, lot D00 138544
Anti IdU antibody	BD Biosciences	Cat# BD 347580
Anti CIdU antibody	Biorad	Cat# OBT0030
Rat anti-BrdU	Abcam	Cat# ab6326
Anti ssDNA antibody	Millipore	Cat# MAB3034
Alexa Fluor 488 Donkey Anti-Rabbit IgG (H+L) Antibody	Thermo Fisher Scientific	Cat# A-21206
Alexa Fluor 488 goat anti-mouse IgG1	Thermo Fisher Scientific	Cat# A-21121
Alexa Fluor 488 goat anti-rat IgG	Thermo Fisher Scientific	Cat# A11007
Alexa Fluor 488 goat anti-mouse IgG2a	Thermo Fisher Scientific	Cat# A21241
Chemicals, and Recombinant Proteins, Culture Media		
DMEM-HG	Thermo Fisher Scientific	Cat#10569010
Knockout DMEM	Life Technologies	Cat# 10829–018
Stemflex	Gibco	Cat# A3349401
5-Iodo-2'-deoxyuridine (IdU)	Sigma Aldrich	Cat# I7125
5-Iodo-2'-deoxyuridine (CldU)	Sigma Aldrich	Cat# C6891
DMSO	Sigma Aldrich	Cat# D2650
PBS	Life Technologies	Cat# 14190–250
TrypLE Express	LifeTechnologies	12605036
Gelatin	Millipore	#ES-006-B
FBS	Atlanta Biologicals	Cat# S11150
Knockout Serum Replacement	Life Technologies	Cat# 10828–028
Glutamax	Thermo Fisher Scientific	Cat# 35050079
MEM NEAA	Life Technologies	Cat# 11140050
PenStrep	Thermo Fisher Scientific	Cat# 15140163
Jetprime	VWR	Cat# 89129–922
Protamine Sulfate	Fisher Scientific	Cat# 0219472905

REAGENT or RESOURCE	SOURCE	IDENTIFIER
Doxycycline	Sigma Aldrich	Cat# D9891
2-mercaptoetahnol	Life Technologies	Cat# 21985–023
LIF	eBioscience	Cat# 34-8521-82
Aphidicolin	Sigma Aldrich	Cat# A0781
Topotecan	Sigma Aldrich	Cat# T2705
Olaparib	Selleckchem	Cat# S1060
Hydroxyurea	Sigma-Aldrich	Cat# H8627–1G
Pyridostatin	Selleck Chemicals	Cat# S7444
Puromycin	Thermo Fisher	Cat# A11138–03
Cell Trace CSFE proliferation dye	Thermo Fisher	Cat# C34554
Propidium Iodide	Millipore	Cat# 537059
HEPES	Sigma Aldrich	Cat# H4034
Fatty acid free BSA	Millipore Sigma	Cat# 126575
Acetic acid	LabChem	Cat# LC101003s
Methanol	Sigma Aldrich	Cat# 322415
Triton X-100	Sigma Aldrich	Cat# T8787
Ethylenediaminetetraacetic acid (EDTA)	Sigma Aldrich	Cat# E6758
Sodium dodecyl sulfate (SDS)	Sigma Aldrich	Cat# L3771
Tris base	Sigma Aldrich	Cat# T1503
NaCl	Sigma-Aldrich	Cat# 71376
MOPS	Sigma-Aldrich	Cat# M1254
$MgCl_2$	Sigma-Aldrich	Cat# M7304
Sucrose	Sigma-Aldrich	Cat# S0389
HCl	Fisher Scientific	Cat# A144sI-212
S1 nuclease	Thermo Fisher Scientific	Cat# 18001–016
Acidic Tyrode’s solution	EMD Millipore	Cat# MR-004-D
Prolong Gold Antifade	Thermo Fisher Scientific	Cat# P10144
Paraformaldehyde	Santa Cruz Biotechnology	Cat# sc-281692
Hoechst33342	Life Technologies	Cat# H3570
Critical Commercial Assays		
Vector Red detection kit	Vector Laboratories	Cat# SK-5100
CytoTune-iPS 2.0 Sendai Reprogramming Kit	Thermo Fisher Scientific	Cat# A16517
RNeasy Mini Kit	Qiagen	Cat# 74104
iScript™ cDNA Synthesis Kit	Bio-RAD	Cat# 1708891
AzuraView™ GreenFast qPCR Blue Mix	Azura Genomics	Cat# AZ-2305
Annexin V-FITC apoptosis detection kit	Sigma Aldrich	Cat# APOAF-20TST
Experimental Models: Cell lines		
293T cells	ATCC	CRL-3216
MEFs: $Brca2^{S3214A/S3214A}$	Jasin lab, Memorial Sloan Kettering Cancer Center. (Lim et al., 2024)	N/A

REAGENT or RESOURCE	SOURCE	IDENTIFIER
MEFs: Brca2$^{+/\Delta 27}$	Jasin lab, Memorial Sloan Kettering Cancer Center. (Lim et al., 2024)	N/A
MEFs: Brca2 $^{\Delta 27/\Delta 27}$	Jasin lab, Memorial Sloan Kettering Cancer Center. (Lim et al., 2024)	N/A
MEFs: Brca2$^{+/S3214A}$	Jasin lab, Memorial Sloan Kettering Cancer Center. (Lim et al., 2024)	N/A
MEFs: Brca1$^{tr/tr}$ Smarcal1$^{+/-}$	This paper	N/A
MEFs: Brca1$^{tr/tr}$ Smarcal1$^{-/-}$	This paper	N/A
MEFs: Brca1$^{tr/tr}$ 53bp1$^{-/-}$	This paper	N/A
MEFs: Brca1$^{tr/tr}$ 53bp1$^{+/-}$	This paper	N/A
MEFs: Smarcal1$^{+/-}$	This paper	N/A
MEFs: Smarcal1$^{-/-}$	This paper	N/A
MEFs: Brca1$^{tr/+}$	This paper	N/A
MEFs: Brca1$^{tr/tr}$	This paper	N/A
MEFs: 53bp1$^{+/-}$	This paper	N/A
MEFs: 53bp1$^{-/-}$	This paper	N/A
MEFs: AABB	This paper	N/A
MEFs: BBCC	This paper	N/A
MEFs: AACC	This paper	N/A
MEFs: AABBCC	This paper	N/A
MEFs: Bard1K607A/+	This paper	N/A
MEFs: Bard1K607A/K607A	This paper	N/A
MEFs: Bard1S563F/+	This paper	N/A
MEFs: Bard1S563F/S563F	This paper	N/A
Abraxas$^{S404A/S404A}$Bach1$^{S994A/S994A}$ iPSC (AABB iPSC)	This paper; Columbia University Medical Center	N/A
Bach1$^{S994A/S994A}$ Ctip$^{S326A/S326A}$ iPSC (BBCC iPSC)	This paper; Columbia University Medical Center	N/A
Abraxas$^{S404A/S404A}$ Ctip$^{S326A/S326A}$ iPSC (AACC iPSC)	This paper; Columbia University Medical Center	N/A
Abraxas$^{S404A/S404A}$Bach1$^{S994A/S994A}$ Ctip$^{S326A/S326A}$ iPSC (AABBCC iPSC)	This paper; Columbia University Medical Center	N/A
Brca1$^{tr/+}$ iPSC	This paper; Columbia University Medical Center	N/A
Brca1$^{tr/tr}$ iPSC	This paper; Columbia University Medical Center	N/A
Brca1$^{tr/tr}$ Smarcal1$^{-/-}$ iPSC	This paper; Columbia University Medical Center	N/A
53bp1$^{-/-}$ iPSC	This paper; Columbia University Medical Center	N/A
Brca1$^{tr/tr}$ iPSC	This paper; Columbia University Medical Center	N/A
Brca1$^{tr/tr}$ 53bp1$^{+/-}$ iPSC	This paper; Columbia University Medical Center	N/A

REAGENT or RESOURCE	SOURCE	IDENTIFIER
Brca1$^{tr/tr}$ 53bp1$^{-/-}$ iPSC	This paper; Columbia University Medical Center	N/A
Human somatic cell line	Columbia University Medical Center. Egli lab repository https://www.eglilab.com/cell-line-repository. (Sui et al., 2021)	#1–023
Experimental Models: Organisms/strains		
Mouse: C57BL/6J	The Jackson Laboratory	RRID: IMSR_JAX:000664
Mouse: Smarcal1$^{+/-, +/-}$	the International Mouse Phenotyping Consortium (IMPC)	N/A
Mouse: Bard1$^{K607A/+, K607A/K607A, S563F/+, S563F/S563F, tr/+}$ (C57BL/6J)	This paper	N/A
Mouse: Brca1tr/tr, tr/+	This paper	N/A
Mouse: Brca1$^{tr/+, tr/tr}$ Smarcal1$^{+/-, -/-}$ (C57BL/6J and 129Sv)	This paper	N/A
Mouse: Brca1$^{tr/+, tr/tr}$53bp1$^{+/-, -/-}$(C57BL/6J and 129Sv)	This paper	N/A
Mouse: 53bp1+/−, −/−	This paper	N/A
Mouse: Abraxas$^{S404A/S404A}$ (C57BL/6J and 129Sv)	This paper	N/A
Mouse: Ctip$^{S326A/S326A}$ (C57BL/6J and 129Sv)	Jackson Laboratories(Reczek et al., 2013)	RRID:IMSR_JAX:036502
Mouse: Bach1$^{S994A/S994A}$ (C57BL/6J and 129Sv)	This paper	N/A
Oligonucleotides		
Primer: 53BP1 Forward: ATGGACCCTACTGGAAGTCAG	This paper	N/A
Primer: 53BP1 Reverse: TTTCTTTGTGCGTCTGGAGATT	This paper	N/A
Primer: GAPDH Forward: GGAGCGAGATCCCTCCAAAAT	This paper	N/A
Primer: GAPDH Reverse: GGCTGTTGTCATACTTCTCATGG	This paper	N/A
Primer: P21 Forward: GCCTTAGCCCTCACTCTGTG	This paper	N/A
Primer: P21 Reverse: AGCTGGCCTTAGAGGTGACA	This paper	N/A
Primer: Beta actin Forward: GGCTGTATTCCCCTCCATCG	This paper	N/A
Primer: Beta actin Reverse: CCAGTTGGTAACAATGCCATGT	This paper	N/A
53BP1-siRNA	Sigma Aldrich	Cat#SASI_Hs01_00024577
Recombinant DNA		
pTet-O-FUW-OSKM	Addgene	Cat# 20321
pFUW-M2rtTA	Addgene	Cat# 20342
pMD2VSVG	Addgene	Cat# 12259
psPax2	Addgene	Cat# 12260
Software and Algorithms		
Prism	GraphPad	https://www.graphpad.com/scientific-software/prism/
Zen confocal imaging and image processing software	Zeiss	https://www.zeiss.com/microscopy/us/products/microscope-software/zen.html
Olympus cellSens imaging and analysis software	Olympus life science	https://www.olympus-lifescience.com/en/software/cellsens

REAGENT or RESOURCE	SOURCE	IDENTIFIER
FlowJo v.10	FlowJo	https://www.flowjo.com/solutions/flowjo/downloads
ImageJ software	ImageJ	https://imagej.net/ij/
OTHER		
40μm cell strainer	Fisher Scientific	Cat# 08-771-1
0.45um PES Syringe Filters	CELLTREAT	Cat# 229749